

Rethink Model Re-Basin and the Linear Mode Connectivity

Xingyu Qu¹ Samuel Horvath¹

Abstract

Recent studies suggest that with sufficiently wide models, most SGD solutions can, up to permutation, converge into the same basin. This phenomenon, known as the model re-basin regime, has significant implications for model averaging. However, current re-basin strategies are limited in effectiveness due to a lack of comprehensive understanding of underlying mechanisms. Addressing this gap, our work revisits standard practices and uncovers the frequent inadequacies of existing matching algorithms, which we show can be mitigated through proper re-normalization. By introducing a more direct analytical approach, we expose the interaction between matching algorithms and re-normalization processes. This perspective not only clarifies and refines previous findings but also facilitates novel insights. For instance, it connects the linear mode connectivity to pruning, motivating a lightweight yet effective post-pruning plug-in that can be directly merged with any existing pruning techniques. Our implementation is available at <https://github.com/XingyuQu/rethink-re-basin>.

1. Introduction and Related Work

Standard deep learning trains a randomly initialized neural network through optimization algorithms like stochastic gradient descent (SGD) to minimize the empirical loss, moving the model downward on the loss landscape and ultimately converging at a “basin”. In the literature, e.g., Neyshabur et al. (2020), the word “basin” roughly refers to a low-loss region around a local minimum and is often regarded to be near-convex. This intuitive concept has spurred a range of research directions aimed at improving practical applications. One notable direction is averaging multiple minima within the same basin to enhance performance while reducing inference and storage costs (Wortsman et al., 2022; Paul

¹Mohamed bin Zayed University of Artificial Intelligence (MBZUAI). Correspondence to: Xingyu Qu, Samuel Horvath <{Xingyu.Qu, Samuel.Horvath}@mbzuai.ac.ae>.

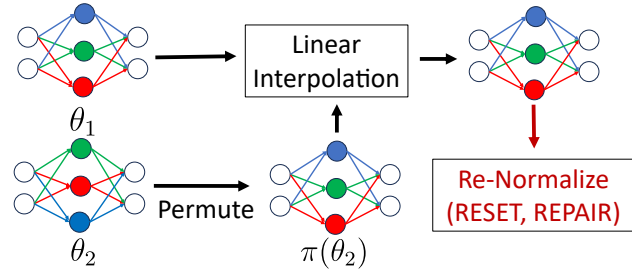


Figure 1. The standard approach in model re-basin.

et al., 2022).

However, there are typically large barriers on the loss landscape between independent SGD solutions (Frankle et al., 2020), and direct model averaging only leads to poor models. Surprisingly, it was recently conjectured (Entezari et al., 2021) that this linear barrier could be eliminated considering the permutation invariance of neural networks. Informally, it hypothesizes that most SGD solutions could be permuted into the same basin, assuming the model is wide enough. Multiple works empirically support this conjecture (Ainsworth et al., 2022; Benzing et al., 2022), where different model-matching algorithms were proposed to discover permutations that can align two networks. Notably, a zero linear barrier, a.k.a *Linear Mode Connectivity (LMC)*, has been achieved between independently trained ResNet20 (He et al., 2016) by Ainsworth et al. (2022). Furthermore, these model re-basin practices were also validated to merge models between different datasets effectively (Ainsworth et al., 2022; Yamada et al., 2023). Despite extensive empirical explorations, existing re-basin strategies unsatisfactorily remain effective in only a limited range of scenarios. It was observed that a significantly large model width was often necessary (Ainsworth et al., 2022), which is impractical and inconsistent with typical approaches. Recently, Jordan et al. (2022) observed that the popular re-basin technique of activation matching is often insufficient to achieve a low barrier between plain models (i.e., without normalization layers) due to the “variance collapse” phenomenon. We attribute these challenges to the limited understanding of the field thus far. While there have been some theoretical efforts (Entezari et al., 2021; Ferbach et al., 2023), they primarily address simpler and more idealized scenarios, lacking practical guidelines for broader application.

Contributions. To tackle this, this work makes the following contributions:

- We conduct the first comprehensive analysis of re-basing independent SGD solutions trained on the same dataset. Our findings reveal that contemporary matching algorithms struggle to identify the optimal permutation. However, certain post-processing techniques effectively enhance these algorithms.
- We introduce a more direct empirical analysis to explain the success of re-basin strategies. This involves (1) using matching algorithms to reduce significant mismatches between models, thereby preserving more knowledge after interpolation, and (2) applying re-normalization to strengthen the remaining information and restore model performance. Our analysis clarifies and improves upon previous results and paves the way for new discoveries.
- Our proposed perspective also links Linear Mode Connectivity (LMC) with pruning. This leads us to develop a lightweight yet effective post-pruning technique that significantly boosts performance and can be integrated seamlessly with any existing pruning framework.

2. Preliminaries

2.1. Linear Mode Connectivity

Definition 2.1 (Loss barrier). Given two models θ_1, θ_2 , and the loss function \mathcal{L} such that $\mathcal{L}(\theta_1) \approx \mathcal{L}(\theta_2)$, the *loss barrier* between the two models is defined as $\max_{\lambda \in [0,1]} \mathcal{L}((1-\lambda)\theta_1 + \lambda\theta_2) - (1-\lambda)\mathcal{L}(\theta_1) - \lambda\mathcal{L}(\theta_2)$.

Definition 2.1 follows Jordan et al. (2022). The symbol λ is also directly used in all of our interpolation plots. For networks with BatchNorm (Ioffe & Szegedy, 2015) layers, it was observed that a statistics reset (Ainsworth et al., 2022) on the interpolated models was often required to maintain the performance, though it remains a mystery why such a process is necessary. Specifically, the running mean and variance in each BatchNorm layer are first reset to default values and then re-accumulated by feeding the entire or a portion of the training dataset to the model. We will simply call this procedure “RESET” hereafter. We say there is a *linear mode connectivity* (LMC) between two models if the loss barrier is closed to 0. A similar barrier definition can be obtained for accuracy. In Entezari et al. (2021), the authors conjectured that LMC generally holds between any pair of models if the permutation invariance of the neural network is taken into account.

2.2. Neural Network Matching

To simplify the explanation, we focus on fully connected feed-forward networks. The statement can be naturally extended to other model architectures. For an L-layer MLP,

$N(x) = N^{(L)}(x)$, where $N^{(i)}(x)$ denotes the output of the i th layer, σ denotes the activation function, W_{i+1} and b_{i+1} are the weights and biases of the $(i+1)$ th layer. The *permutation invariance* of neural network indicates that if we apply a permutation P to the output of the last layer, i.e., $N^{(i)}(x) \leftarrow PN^{(i)}(x)$, the output of the network can be the same once we permute the parameters in the next layer accordingly: $W_{i+1} \leftarrow W_{i+1}P^T$, since it holds that $P^TP = I$. Permuting the output of the layer is also equivalent to permuting the parameters in the layer: $W_i \leftarrow PW_i$, $b_i \leftarrow Pb_i$. Therefore, one can obtain a functionally equivalent network $N'(x) = N(x)$ by applying permutations to the parameters $\theta' = \pi(\theta)$.

Neural network matching aims to align two networks through the permutation invariances in the parameter space. We adopt two widely used matching algorithms in the literature: weight matching (Ainsworth et al., 2022) and activation matching (Ainsworth et al., 2022; Jordan et al., 2022). Briefly, given two networks N_1 and N_2 , weight matching seeks the permutation minimizing the distance between the parameters: $\pi^* = \operatorname{argmin}_{\pi} \|\theta_1 - \pi(\theta_2)\|$, while activation matching minimizes the distance between intermediate activations of each hidden layer: $\pi^* = \operatorname{argmin}_{\pi} \sum_i \|N_1^{(i)}(x) - \pi(N_2)^{(i)}(x)\|$. Notably, we found that the performance of activation matching can degrade due to insufficient numerical precisions when accumulating and matching the activations. The method proposed in Jordan et al. (2022) generally outperforms the one in Ainsworth et al. (2022) while the only difference is how they accumulate the activations in their implementations. We address this by combining both implementations to obtain a high-precision yet computationally cheap approach. Detailed discussions are provided in Appendix D.2.

2.3. Experimental Setup

Following standard results in prior works, we study re-basing independent SGD solutions trained on the same image classification datasets: MNIST (Deng, 2012), CIFAR-10/CIFAR-100 (Krizhevsky et al., 2009). Pruning results on ImageNet (Deng et al., 2009) are also provided. We explore various network architectures, including the fully connected network (MLP), VGG (Simonyan & Zisserman, 2014), and ResNet, with different depth, width, and the inclusion of BatchNorm, LayerNorm (Ba et al., 2016), and no normalization. ResNet with Fixup (Zhang et al., 2019) initialization is also considered. We follow the standard setup for network training (Frankle et al., 2020; He et al., 2016). We train the VGGS and ResNets for 160 epochs with weight decay 10^{-4} . Unless otherwise specified, the learning rate is initialized at 0.1 and reduced by a factor of 10 at iteration 32,000 and 48,000. A linear warmup or cosine decay is also adopted in some settings to ensure smooth training. Complete experimental details are provided in Appendix C.

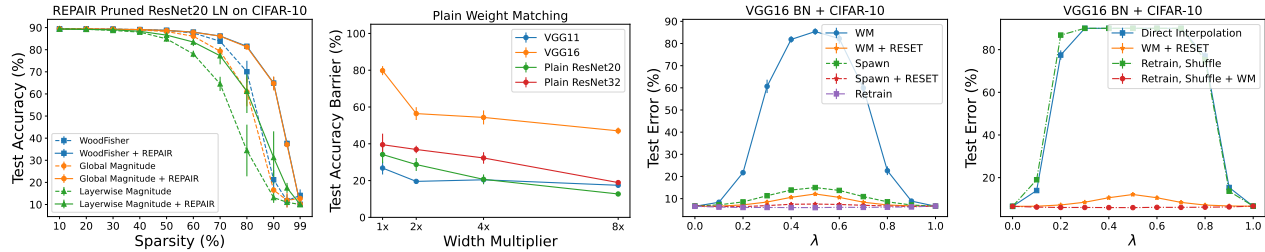


Figure 2. (A) Apply REPAIR to ResNet20 LN (LayerNorm) after pruning on CIFAR-10. (B) Performance of weight matching on plain models. (C) & (D) Comparison between re-basin and the same basin scenario. “Shuffle” refers to applying a random permutation to the basin. WM: Weight Matching.

3. Rethink the “Re-Basin” Conjecture

This section revisits the standard practice in model re-basin from the conventional basin perspective. The results suggest that current matching algorithms struggle to identify the optimal permutation. However, we show that certain post-processing techniques effectively enhance these existing algorithms.

3.1. Importance of Re-Normalization

Jordan et al. (2022) observed activation matching was insufficient to achieve low barriers on plain VGG and ResNet, emphasizing the importance of re-normalization, e.g., RESET for models with BatchNorm or utilizing models with LayerNorm which performs running-time normalization. The same observation was drawn in our experiments using the weight-matching algorithm. We also noticed that the barrier decreased as we increased the model width while the reduction speed was relatively slow, e.g., less than 10% improvement was seen by increasing width from $2\times$ to $8\times$ on VGG16. We report the test accuracy barrier when re-basing different variants of VGG and ResNet trained on CIFAR-10 in Figure 2 (B).

However, to our knowledge, previous literature did not provide strong evidence that re-normalization is necessary when averaging models located in the same basin. To investigate this, we conducted multiple experiments to compare the two scenarios.

3.2. Comparison to the Same Basin Scenario

Prior works (Frankle et al., 2020; Fort et al., 2020) produce solutions located in the same basin in a “spawning” style: a parent model is firstly trained for several epochs, then multiple child models are created from the current pre-trained checkpoint and are independently trained for the rest training budget. We replicate the spawning experiments using VGG16 BN and ResNet20 on CIFAR-10. According to Frankle et al. (2020), we pre-train VGG16 BN for one epoch to obtain a test accuracy barrier within 10% - 15% between two converged child models. This value is simi-

lar to that between two independently trained VGG16 BN after permutation and RESET, creating a fair comparison. Similarly, we pre-train ResNet20 for two epochs. Surprisingly, we observe that a small barrier of around 15% can be achieved even without RESET in the spawning experiment, while the re-basin merely achieves a barrier of over 75%, as shown in Figure 2 (C). After applying RESET, the spawning barrier further falls below 1%. It suggests that RESET is not necessary for averaging models in the same basin. This significant difference also raises doubts about whether the current matching algorithms truly permute two models into the same basin.

For a better comparison, we consider a more accurate and lightweight approach to approximate the same basin scenario. Motivated by approaches in Izmailov et al. (2018); Garipov et al. (2018), we create a copy of one pre-trained solution and retrain this copy for several epochs using a large learning rate followed by a small learning rate to produce a different solution close to the original one. Details are reported in Appendix E.2. Notably, we observed the LMC (even w/o RESET), as visualized in Figure 2 (C). Consistent with results in early works (Neyshabur et al., 2020), this indicates the two solutions are located in the same nearly convex basin. Using the same setup, we further measure the ability of current matching algorithms to identify a certain basin. After obtaining two solutions θ_1 and θ_2 located in the same basin, a random permutation is applied: $\theta_1 \rightarrow \pi(\theta_1)$. We then perform the matching algorithms to align $\pi(\theta_1)$ and θ_2 . We verify if π' , the permutation returned by the matching algorithm precisely recovers the original θ_1 , i.e., if $\pi' = \pi^{-1}$. Different from the independent training + re-basin scenario, we observed that both matching strategies can recover the basin exactly, as shown in Figure 2 (D). Meanwhile, we observed the distance between models in the same basin was significantly smaller than the one between two independent solutions after matching.

In summary, these results highlight a noteworthy distinction between the same basin and the current re-basin scenario, raising doubts about whether the matching algorithms truly permute independent solutions into the same basin.

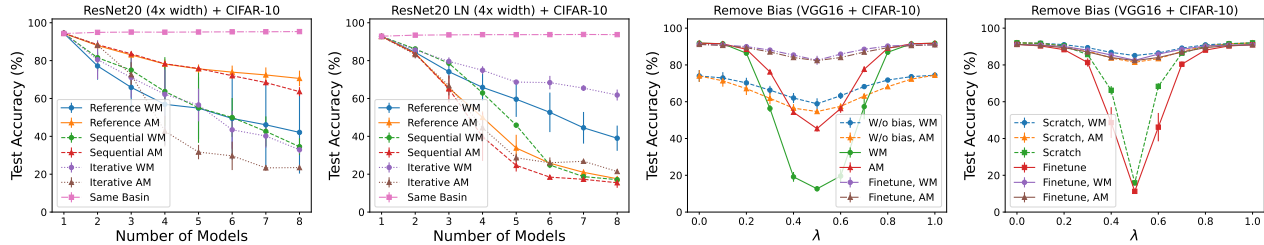


Figure 3. (A) & (B) Multiple model matching. The test accuracy of the average model is reported. AM: Activation Matching. (C) Removing biases from pre-trained models followed by fine-tuning significantly reduces the barrier. (D) Compare removing biases at initialization and after training.

3.3. Instability in Multiple Network Merging

This section provides more evidence that current practice does not seem to re-base independent solutions into the same basin. Yunis et al. (2022) demonstrate that SGD trajectories will likely converge to a convex basin by finding a convex hull of low loss between child solutions in the spawning experiment. Regarding the independent training, Csizsárik et al. (2023) reports the existence of a transitivity property: two models permuted to match a third reference model are also connected in linear mode. Consequently, averaging models re-based to the same basin should also benefit.

To verify this corollary, we design two natural multiple-matching regimes: *reference matching* and *sequential matching*. To match n independently trained networks $\theta_1, \theta_2, \dots, \theta_n$, the reference matching selects θ_1 as the reference model and matches all other models to it; while the sequential matching sequentially matches θ_{i+1} to $\hat{\theta}_i$ where $\hat{\theta}_i$ is the permuted θ_i from the last matching and we define $\hat{\theta}_1 = \theta_1$. Ainsworth et al. (2022) also derived an iterative algorithm but only considered merging MLPs trained on MNIST through weight matching. In every iteration, this *iterative matching* performs n reference matching sequentially where one model is randomly selected (without replacement) to be permuted and match the center of the rest models. The algorithm terminates once it converges.

The three mentioned multi-matching approaches are evaluated to align independent solutions trained on CIFAR-10. Results of ResNet20 and ResNet20 LN are shown in Figure 3 (A) & (B). Unexpectedly, the performance of the average model decreases rapidly as we increase the number of models in all matching regimes. Although the more advanced iterative matching performs tens of more matching operations, it only attains a slight or zero enhancement compared to the trivial reference matching. This unstable performance might be attributed to the fact that it often couldn't converge within the given time (several hours), and hence, we manually terminated the algorithm after 30 iterations. We also evaluated direct multiple model averaging in the same basin scenario to compare. We adopted the re-

training strategy introduced in the last section to produce the models. The results (Figure 3 (A) & (B), in pink) show that the average model consistently outperforms all end models regardless of the number of models.

In conclusion, this instability in the multi-re-basin experiment (in contrast to the robust merging performance within the same basin) provides another contradiction to the conventional re-basin view.

3.4. Intriguing Property of Biases

In our exploration, an intriguing observation was drawn: removing biases from the model has a similar effect to re-normalization in decreasing the post-re-basin barrier. As shown in Figure 3 (C), the midpoint between two independently trained VGG16 remained to perform as a random guess after weight matching. Surprisingly, by simply removing the biases in each layer from models, the midpoint performance suddenly improved, albeit the end model became worse and hence got out of the basin. We then fine-tuned the end models to recover a training accuracy above 90%. It turned out that applying the same permutation maintained the test accuracy barrier to be as low as 8%. Results were similar by applying new permutations found without considering biases. The same small barrier can also be obtained by training two models without biases from scratch, as visualized in Figure 3 (D). On average, removing the biases significantly decreases the weight matching barrier from 79.19% to 8.54% and the activation matching barrier from 46.49% to 8.71%. We observed this phenomenon to be consistent across different models and datasets. In addition, removing biases and re-normalization led to a similar level of reduction, see Appendix E.5

This surprising observation, along with other results we have presented, suggests that the small barrier observed in prior works may not solely be due to geometrically aligning models to the same basin. Instead, it appears to be significantly aided by certain beneficial techniques, such as re-normalization.

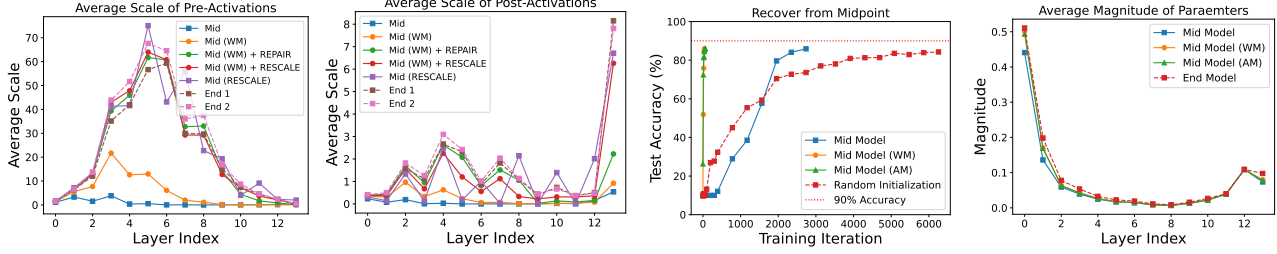


Figure 4. (A) & (B) Average scale of pre-ReLU and post-ReLU activations in each layer. (C) Test accuracy of the midpoint model during retraining until achieving a training accuracy of 90%. (D) Average magnitude of parameters in each layer. After matching, the reduction in magnitude decreased, demonstrating the effect of knowledge retention. Results are evaluated on VGG16 trained on CIFAR-10.

Table 1. Ablation to REPAIR. The first line records the test accuracy of the original post-weight-matching midpoint model.

Variant	Test Accuracy
-	14.22 ± 2.27 %
REPAIR	75.1 ± 4.09 %
RESCALE	84.32 ± 0.77 %
RESCALE (average)	78.18 ± 0.88 %
RESHIFT	10 %

A similar discussion is shown by Wang et al. (2022). There, the authors considered the interpolation between a random initialization and the SGD solution and revealed that the shape of the interpolation plot depends heavily on the last-layer biases and is not necessarily connected to the general geometric property of loss landscape. Indeed, their observation can also be connected to the study of LMC, discussed in Appendix E.5.

4. Matching and Re-Normalization: An Empirical Perspective

In the previous section, we revisited standard practices and discovered that models were not re-based into the same basin as previously thought. Instead, we found that re-normalization plays a pivotal role. Building on this insight, this section aims to provide a clearer analysis of past successes and failures, guiding and improving current practices.

4.1. Effect of REPAIR: Rescaling

Our investigation starts by exploring the effect of the re-normalization. Generally, previous re-normalization was achieved through three approaches: employing models with BatchNorm and performing RESET, using models with LayerNorm, or applying REPAIR (Jordan et al., 2022) to plain models. Given the limited understanding of BatchNorm and LayerNorm, our primary emphasis is on the last scenario, but the insights we obtained turned out to be universal.

REPAIR was proposed to tackle the issue of “variance collapse”: the hidden activation variances significantly decrease in the interpolated models, and this reduction be-

comes more pronounced in deeper layers. Eventually, it leads to nearly constant activations in the output layer, resulting in model performance degradation. This issue was observed to become less severe in models with LayerNorm and more negligible in models with BatchNorm after applying RESET. This motivated the authors to leverage the idea of running statistics correction in RESET to improve interpolation between plain models. Given two networks N_1 , N_2 and the interpolated network N_α of which parameters $\theta_\alpha = (1 - \alpha) \cdot \theta_1 + \alpha \cdot \theta_2$, REPAIR corrects the channel-wise statistics for all selected layers $N_\alpha^{(i)}$ in N_α based on the corresponding layers $N_1^{(i)}$, $N_2^{(i)}$ from the end models:

$$\text{REPAIR: } N_\alpha^{(i)}(x) \leftarrow \frac{N_\alpha^{(i)}(x) - \mu_\alpha}{\sigma_\alpha} \cdot w_\alpha + b_\alpha,$$

where x , $N_\alpha^{(i)}(x)$ is the input and pre-activation of $N_\alpha^{(i)}$, $w_\alpha = (1 - \alpha) \cdot \mu_1 + \alpha \cdot \mu_2$ is the goal running mean, $b_\alpha = (1 - \alpha) \cdot \sigma_1 + \alpha \cdot \sigma_2$ is the goal running standard deviation, and μ , σ is the channel-wise mean and standard deviation of the layer output. The subscript refers to which model the statistics belong to. This process repairs the hidden running means and variances in the interpolated model. Our first question is whether the two corrections are equivalently important to the success of REPAIR. Two variants of REPAIR are proposed for this purpose:

$$\text{RESCALE: } N_\alpha^{(i)}(x) \leftarrow \frac{N_\alpha^{(i)}(x)}{\sigma_\alpha} \cdot w_\alpha,$$

$$\text{RESHIFT: } N_\alpha^{(i)}(x) \leftarrow N_\alpha^{(i)}(x) - \mu_\alpha + b_\alpha.$$

It’s noteworthy that although RESHIFT did not explicitly recover the running variance, the correction of statistics still might alleviate the issue (discussed in Appendix F.1). We assess the performance of each method in repairing the post-matching midpoint model between two independently trained plain models. Results of VGG16 trained on CIFAR-10 are shown in Table 1.

Surprisingly, we observed that RESCALE reduced the barrier by an additional 9% on average compared with REPAIR, while RESHIFT degraded the performance. Remarkably,

RESCALE demonstrated comparable performance to REPAIR even when only provided with the average standard deviation $\bar{w}_\alpha = \text{mean}(w_\alpha) \cdot \mathbf{1}$ in each layer. Across all the models and datasets considered, RESCALE consistently performs no worse than REPAIR. Therefore, it suggests that rescaling the intermediate activation is the key to the success of REPAIR. We visualize the effect of rescaling by comparing the average pre-activation scale in each layer. As depicted in Figure 4 (A) & (B), the hidden activation scale dramatically decreases after the interpolation, slightly increases after performing matching, and is eventually recovered after an additional REPAIR or RESCALE. Notably, the scale-up in the activation scale also increases the activation variance, and the effect is then propagated to the post-activation statistics due to the piece-wise linearity of ReLU, alleviating the variance collapse.

To conclude, the above results reveal that the success of REPAIR mainly depends on re-scaling up activations in the interpolated model to alleviate the variance collapse. It is also noteworthy that the performance of REPAIR in this section is worse than the one in Jordan et al. (2022). We will revisit and explain this difference in Sec. 4.3.

4.2. Effect of Matching: Knowledge Retained

An appealing question suddenly arises from the conclusion in the last section: *would the barrier decrease the same way if we rescale the activation in interpolated models but without matching?* Unfortunately, the answer was already reported to be negative by Jordan et al. (2022), where no obvious improvement was observed. Following the same experimental setup as in the last section, we found similar results that the test accuracy of the midpoint model after REPAIR and RESCALE is only 10.01% and 12.87%, respectively. To understand the crucial effect of matching here, we carefully examined the statistics in the model. Surprisingly, we noticed that although the pre-activation statistics were recovered within the model, there was no obvious increase in post-activation scales, as shown in Figure 4 (B). We discovered that the underlying reason for this issue was that some neurons became inactive during forward calculation, consistently outputting zeros, which remained unaffected by rescaling. This problem was notably mitigated after matching.

As a typical form of feature learning, the internal representations of neural networks are often regarded as new features extracted by the model (LeCun et al., 2015). In this sense, the above observations suggest that some information is permanently lost in the interpolated model and can't be recovered by a single post-re-normalization. Matching helps to retain some information that the re-normalization can amplify to restore model prediction. As shown in Figure 4 (A), the activation scale already partially recovers after a single matching. Meanwhile, the quantity of information stored

in the model can also be directly measured by its performance, which improves after matching. However, there are cases where an obvious improvement is only obtained after re-normalization. To tackle this, we derive a new approach that measures the retained information. We measure how many steps the model requires to reach high performance. Specifically, we first obtained the midpoint model between two independent solutions before and after matching. The model was then retrained with $\text{lr} = 0.01$ until the training accuracy reached 90%. We report the dynamics of test accuracy when conducting experiments on plain VGG16 in Figure 4 (C). Notably, although the initial accuracy after weight matching is as low as 10%, it only requires around 60 mini-batches to achieve 90% training accuracy, significantly faster than training from scratch or the original midpoint model. Meanwhile, there is no decrease in the generalizability of the model. Similar results hold for the activation matching and other model architectures and datasets. This substantial difference further corroborates our claim.

We also found an intriguing analogy between model pruning and LMC, explaining why matching can help retain information. Extensive early works on magnitude-based pruning (Han et al., 2015; Li et al., 2016) reveal that the parameter magnitude can reflect how much information is stored there. Recently, Csiszárík et al. (2023) introduced the concept of mode combinability. They propose that a high-performing network, linearly interpolated between two matched models, can be achieved on a parameter-wise basis if network-wide LMC holds. We notice that a standard unstructured magnitude pruning also produces a parameter-wise interpolated network. Consider performing the magnitude pruning \mathcal{M} to network θ to obtain $\mathcal{M}(\theta)$. For the unpruned (u.p.) sub-network, we have $\mathcal{M}(\theta)_{u.p.} = 0.5 \cdot \theta_{u.p.} + 0.5 \cdot \mathcal{M}(\theta)_{u.p.}$, and for the pruned part we have $\mathcal{M}(\theta)_p = 0 \cdot \theta_p + 1 \cdot \mathcal{M}(\theta)_p$, see Figure 35. The unpruned part represents the interpolation after the perfect re-basin by weight matching and retains all knowledge stored in these important weights, while the pruned part is a mild case of mismatch where less important knowledge is removed, but no additional noise is introduced. Therefore, one can prune most of the parameters with small magnitudes in the model while maintaining the performance, but the model immediately degrades once large parameters are removed. In practice, the weight-matching algorithm approximates this by reducing weight discrepancies between models, as illustrated in Figure 4 (B) & (D). This suggests that achieving a perfect re-basin might not be necessary, provided that sufficient relevant knowledge is retained and noise is minimized. Similarly, this principle can be applied to activation matching by linking the scale of hidden activations to the information contained in those features.

In summary, the discussions so far eventually come to the following explanation:

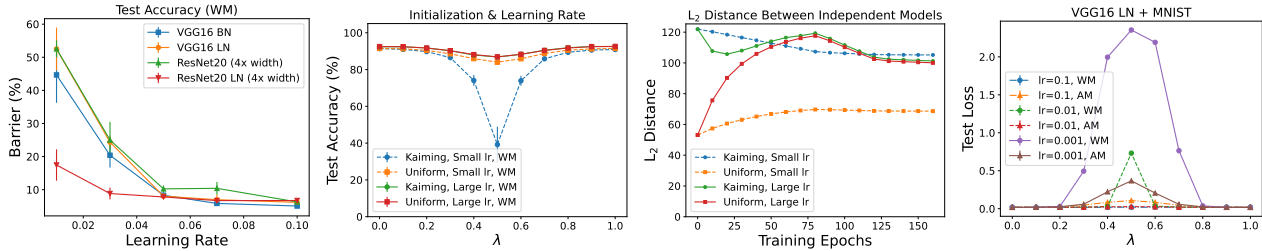


Figure 5. (A) The effect of utilizing a large learning rate in reducing post-matching barriers. (B) Sensitivity to initialization when trained with a small learning rate. (C) Dynamics of distance between independent models during training. (D) Performance of matching between VGG16 LNs trained on MNIST with different values of learning rate.

Conjecture 4.1. *Current success in “re-basin” two independently trained models can be explained as:*

- (1) *Matching algorithms avoid severe mismatch on important parameters, e.g., parameters with large magnitudes or important hidden activations, retaining more information in the interpolated width.*
- (2) *Re-normalization strategies amplify the remaining information and eventually recover the model performance.*

We have identified this as a universal mechanism to enhance model performance. An example is presented in Sec. 5, demonstrating its application in improving pruned networks. This explanation, more direct than the basin view, effectively guides performance enhancements, as evidenced in the remainder of this paper.

4.3. Two Beneficial Implicit Biases

Conjecture 4.1 underscores the importance of retaining information in the interpolated model. A straightforward approach to achieve this is to discover a better permutation that minimizes mismatches between end models. However, this task is notably intricate; for instance, weight matching is known (Ainsworth et al., 2022) to be an NP-hard problem.

Large Learning Rate. In the last section, we revealed an analogy between pruning and LMC. In pruning, the performance of the pruned model is positively correlated with the identification and retention of important weights, as well as the model’s intrinsic sparsity. If the model is inherently more sparse, i.e., the learned knowledge is concentrated in a small portion, it suffices to ensure this subset of weights remains unaffected. It’s noteworthy that the same logic applies to matching. The performance of interpolated models can be guaranteed once those important weights are correctly aligned, and the alignment becomes more attainable if there are merely a small fraction of important weights.

A recent work (Andriushchenko et al., 2023b) reveals that SGD with a large step decay learning rate implicitly regularizes the model towards a sparser solution. Therefore, we expect that models trained with a larger step size inherently have a smaller barrier. To verify this, we conducted

extensive experiments on different networks and datasets, with one result reported in Figure 5 (A). As expected, it was observed that the performance of interpolated models kept improving as we increased the learning rate; e.g., a significant 40% decrease in the test accuracy barrier was observed on VGG16 LN. To ensure that the observed improvements were not merely due to better performance from models trained with higher learning rates, we further trained at the higher learning rates until model performance fell below the models trained with lower learning rates. As discussed in Appendix F.5, it was observed that the post-matching barrier in the former case is still significantly smaller than the latter. *In summary, it suggests that the implicit bias of large learning rates is beneficial to decrease the barrier in model re-basin.*

In Ainsworth et al. (2022), the authors reported some failed cases of the standard practice, including matching MNIST MLPs trained with a too-low learning rate and matching VGG16 LN trained on MNIST. While the former observation is consistent with our findings, we found that the second failure was also attributed to a small training learning rate, illustrated in Figure 5 (D). In our experiments, another issue caused by small learning rates was found. Specifically, we replicated the experiment in Ainsworth et al. (2022) to match two independently trained VGG16 LN, where we changed the initial learning rate from 0.1 to 0.01. Two standard initialization methods were considered: Kaiming (normal) initialization and (Kaiming) uniform initialization (He et al., 2015). We found while the two initialization strategies lead to solutions with similar performances, the post-weight-matching barrier between Kaiming initialized solutions was over 40% larger than the barrier between uniformly initialized solutions. This difference suddenly disappeared after we adopted a larger learning rate. Similar observations were drawn on the activation matching. Test accuracy results are shown in Figure 5 (B). After careful examination, we found that Kaiming initialization samples elements from a distribution with a larger variance, and hence, the initial distance between two independent models is larger. When trained with small learning rates, models tend to converge towards solutions close to the initialization (Andriushchenko et al.,

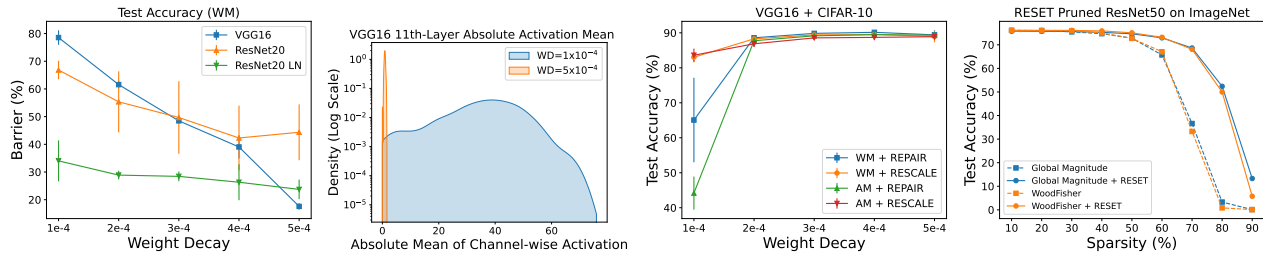


Figure 6. (A) The effect of utilizing a large weight decay in reducing post-matching barriers. (B) The compression effect of large weight decay. (C) Compare performances of REPAIR and RESCALE on models trained with different values of weight decay. (D) Apply RESET to pruned ResNet50 on ImageNet.

2023b), maintaining the large distance between the final solutions, making it challenging or even impossible to discover a permutation for effective matching. On the other hand, the implicit bias of large learning rates mitigates the impact of initialization. We report the ℓ_2 distance between independent models during training in Figure 5 (C).

Large Weight Decay. The motivation for adopting large learning rates can be interpreted as saving more information in each successful match by directly concentrating learned knowledge into a small fraction of weights. Conversely, this can also be achieved by reducing the information loss during each mismatch. One simple idea is to compress all the weights and hidden activations into a small region, and hence, the severeness of mismatch is bounded. This inspires us to verify if training with large weight decay, which exactly does this role (see Figure 6 (B)), can also lead to smaller barriers. It turned out that increasing the weight decay within a threshold kept decreasing the barrier, as depicted in Figure 6 (A), supporting our intuition. We also conducted ablation experiments in Appendix F.6 to demonstrate the improvement of end models did not trivially bring this benefit.

Recall that the performance of REPAIR reported in Sec. 4.1 is worse than the one shown in Jordan et al. (2022). We found that this difference was brought by the choice of weight decay 10^{-4} in our experiments. We report the mid-point test accuracy when training with different values of weight decay in Figure 6 (C). A significant improvement in REPAIR was drawn right after doubling the weight decay regularization. We hypothesize this is because a larger weight decay forces the running statistics of each channel to be similar in value, hence also alleviating the detriment of a mismatch in REPAIR. Notably, our RESCALE was observed to be more robust and can serve as a better solution in this scenario.

5. A Novel Pruning Technique

In Section 4.2, our analysis provides a new perspective: standard network pruning can be seen as a form of parameter-wise linear interpolation. Inspired by this analogy, we ex-

plored the possibility of repairing pruned models through re-normalization. Our experiments spanned various models, datasets, and pruning methods, including global/layerwise magnitude pruning (Han et al., 2015), diagonal-Fisher pruning, and WoodFisher (Singh & Alistarh, 2020) pruning, a recent state-of-the-art method. Remarkably, we found affirmative results across all tests. Post-pruning, we applied a RESET to models with BatchNorm and a REPAIR to plain models or those with LayerNorm. As Figures 2 (A) and 6 (D) illustrate, this simple post-pruning step markedly enhanced model performance after a one-shot pruning, such as a roughly 50% test accuracy increase in ResNet50 + ImageNet at 80% sparsity. This technique requires minimal data (often just one batch) for the estimation of model statistics, making it exceptionally cost-effective. Moreover, the additional BatchNorm parameters in REPAIR can be merged into preceding layers, further reducing complexity. This is particularly advantageous in resource-constrained environments like federated learning on end devices. Besides one-shot pruning, this method seamlessly integrates with any existing pruning strategy. Interestingly, we observed that the performance gap between basic global magnitude pruning and time-intensive WoodFisher pruning disappears after REPAIR. More detailed results and discussions are provided in Appendix G.

6. Conclusion

In summary, this work provides a thorough revisit into the standard re-basin practice and obtains novel insights from two different aspects, unveiling that current matching algorithms fail to identify the optimal permutation but succeed in retaining some information that is amplified by the re-normalization and recover the model performance. The novel qualitative and quantitative analysis has strengths in explaining and improving previous results and guiding new findings. It also connects the LMC to pruning, inspiring a lightweight yet effective post-pruning plug-in that can be directly merged with any existing pruning techniques.

References

- Achille, A., Rovere, M., and Soatto, S. Critical learning periods in deep networks. In *International Conference on Learning Representations*, 2018.
- Adilova, L., Fischer, A., and Jaggi, M. Layerwise linear mode connectivity. *arXiv preprint arXiv:2307.06966*, 2023.
- Ainsworth, S. K., Hayase, J., and Srinivasa, S. Git re-basin: Merging models modulo permutation symmetries. *arXiv preprint arXiv:2209.04836*, 2022.
- Andriushchenko, M., D’Angelo, F., Varre, A., and Flammarion, N. Why do we need weight decay in modern deep learning? *arXiv preprint arXiv:2310.04415*, 2023a.
- Andriushchenko, M., Varre, A. V., Pillaud-Vivien, L., and Flammarion, N. Sgd with large step sizes learns sparse features. In *International Conference on Machine Learning*, pp. 903–925. PMLR, 2023b.
- Ba, J. L., Kiros, J. R., and Hinton, G. E. Layer normalization. *arXiv preprint arXiv:1607.06450*, 2016.
- Benton, G., Maddox, W., Lotfi, S., and Wilson, A. G. G. Loss surface simplexes for mode connecting volumes and fast ensembling. In *International Conference on Machine Learning*, pp. 769–779. PMLR, 2021.
- Benzing, F., Schug, S., Meier, R., Von Oswald, J., Akram, Y., Zucchet, N., Aitchison, L., and Steger, A. Random initialisations performing above chance and how to find them. *arXiv preprint arXiv:2209.07509*, 2022.
- Csiszárík, A., Kiss, M. F., Kőrösi-Szabó, P., Muntag, M., Papp, G., and Varga, D. Mode combinability: Exploring convex combinations of permutation aligned models. *arXiv preprint arXiv:2308.11511*, 2023.
- Deng, J., Dong, W., Socher, R., Li, L.-J., Li, K., and Fei-Fei, L. Imagenet: A large-scale hierarchical image database. In *2009 IEEE conference on computer vision and pattern recognition*, pp. 248–255. Ieee, 2009.
- Deng, L. The mnist database of handwritten digit images for machine learning research [best of the web]. *IEEE signal processing magazine*, 29(6):141–142, 2012.
- Draxler, F., Veschini, K., Salmhofer, M., and Hamprecht, F. Essentially no barriers in neural network energy landscape. In *International conference on machine learning*, pp. 1309–1318. PMLR, 2018.
- Entezari, R., Sedghi, H., Saukh, O., and Neyshabur, B. The role of permutation invariance in linear mode connectivity of neural networks. *arXiv preprint arXiv:2110.06296*, 2021.
- Ferbach, D., Goujaud, B., Gidel, G., and Dieuleveut, A. Proving linear mode connectivity of neural networks via optimal transport. *arXiv preprint arXiv:2310.19103*, 2023.
- Fisher, R. A. Theory of statistical estimation. In *Mathematical proceedings of the Cambridge philosophical society*, volume 22, pp. 700–725. Cambridge University Press, 1925.
- Fort, S., Dziugaite, G. K., Paul, M., Kharaghani, S., Roy, D. M., and Ganguli, S. Deep learning versus kernel learning: an empirical study of loss landscape geometry and the time evolution of the neural tangent kernel. *Advances in Neural Information Processing Systems*, 33: 5850–5861, 2020.
- Frankle, J. Revisiting” qualitatively characterizing neural network optimization problems”. *arXiv preprint arXiv:2012.06898*, 2020.
- Frankle, J. and Carbin, M. The lottery ticket hypothesis: Finding sparse, trainable neural networks. *arXiv preprint arXiv:1803.03635*, 2018.
- Frankle, J., Dziugaite, G. K., Roy, D., and Carbin, M. Linear mode connectivity and the lottery ticket hypothesis. In *International Conference on Machine Learning*, pp. 3259–3269. PMLR, 2020.
- Freeman, C. D. and Bruna, J. Topology and geometry of half-rectified network optimization. *arXiv preprint arXiv:1611.01540*, 2016.
- Garipov, T., Izmailov, P., Podoprikin, D., Vetrov, D. P., and Wilson, A. G. Loss surfaces, mode connectivity, and fast ensembling of dnns. *Advances in neural information processing systems*, 31, 2018.
- Goodfellow, I. J., Vinyals, O., and Saxe, A. M. Qualitatively characterizing neural network optimization problems. *arXiv preprint arXiv:1412.6544*, 2014.
- Gotmare, A., Keskar, N. S., Xiong, C., and Socher, R. Using mode connectivity for loss landscape analysis. *arXiv preprint arXiv:1806.06977*, 2018.
- Han, S., Pool, J., Tran, J., and Dally, W. Learning both weights and connections for efficient neural network. *Advances in neural information processing systems*, 28, 2015.
- He, K., Zhang, X., Ren, S., and Sun, J. Delving deep into rectifiers: Surpassing human-level performance on imagenet classification. In *Proceedings of the IEEE international conference on computer vision*, pp. 1026–1034, 2015.

- He, K., Zhang, X., Ren, S., and Sun, J. Deep residual learning for image recognition. In *Proceedings of the IEEE conference on computer vision and pattern recognition*, pp. 770–778, 2016.
- Iharcó, G., Ribeiro, M. T., Wortsman, M., Gururangan, S., Schmidt, L., Hajishirzi, H., and Farhadi, A. Editing models with task arithmetic. *arXiv preprint arXiv:2212.04089*, 2022.
- Imfeld, M., Graldi, J., Giordano, M., Hofmann, T., Anagnostidis, S., and Singh, S. P. Transformer fusion with optimal transport. *arXiv preprint arXiv:2310.05719*, 2023.
- Ioffe, S. and Szegedy, C. Batch normalization: Accelerating deep network training by reducing internal covariate shift. In *International conference on machine learning*, pp. 448–456. pmlr, 2015.
- Izmailov, P., Podoprikin, D., Garipov, T., Vetrov, D., and Wilson, A. G. Averaging weights leads to wider optima and better generalization. *arXiv preprint arXiv:1803.05407*, 2018.
- Jordan, K., Sedghi, H., Saukh, O., Entezari, R., and Neyshabur, B. Repair: Renormalizing permuted activations for interpolation repair. *arXiv preprint arXiv:2211.08403*, 2022.
- Juneja, J., Bansal, R., Cho, K., Sedoc, J., and Saphra, N. Linear connectivity reveals generalization strategies. *arXiv preprint arXiv:2205.12411*, 2022.
- Krizhevsky, A., Hinton, G., et al. Learning multiple layers of features from tiny images. 2009.
- LeCun, Y., Bengio, Y., and Hinton, G. Deep learning. *nature*, 521(7553):436–444, 2015.
- Li, B., Wu, B., Su, J., and Wang, G. Eagleeye: Fast sub-net evaluation for efficient neural network pruning. In *Computer Vision—ECCV 2020: 16th European Conference, Glasgow, UK, August 23–28, 2020, Proceedings, Part II 16*, pp. 639–654. Springer, 2020.
- Li, H., Kadav, A., Durdanovic, I., Samet, H., and Graf, H. P. Pruning filters for efficient convnets. *arXiv preprint arXiv:1608.08710*, 2016.
- Lubana, E. S., Bigelow, E. J., Dick, R. P., Krueger, D., and Tanaka, H. Mechanistic mode connectivity. In *International Conference on Machine Learning*, pp. 22965–23004. PMLR, 2023.
- Marcel, S. and Rodriguez, Y. Torchvision the machine-vision package of torch. In *Proceedings of the 18th ACM international conference on Multimedia*, pp. 1485–1488, 2010.
- McMahan, B., Moore, E., Ramage, D., Hampson, S., and y Arcas, B. A. Communication-efficient learning of deep networks from decentralized data. In *Artificial intelligence and statistics*, pp. 1273–1282. PMLR, 2017.
- Mohtashami, A., Jaggi, M., and Stich, S. U. Special properties of gradient descent with large learning rates. In *International Conference on Machine Learning*, pp. 25082–25104. PMLR, 2023.
- Nagarajan, V. and Kolter, J. Z. Uniform convergence may be unable to explain generalization in deep learning. *Advances in Neural Information Processing Systems*, 32, 2019.
- Neyshabur, B., Sedghi, H., and Zhang, C. What is being transferred in transfer learning? *Advances in neural information processing systems*, 33:512–523, 2020.
- Paszke, A., Gross, S., Massa, F., Lerer, A., Bradbury, J., Chanan, G., Killeen, T., Lin, Z., Gimelshein, N., Antiga, L., et al. Pytorch: An imperative style, high-performance deep learning library. *Advances in neural information processing systems*, 32, 2019.
- Paul, M., Chen, F., Larsen, B. W., Frankle, J., Ganguli, S., and Dziugaite, G. K. Unmasking the lottery ticket hypothesis: What’s encoded in a winning ticket’s mask? *arXiv preprint arXiv:2210.03044*, 2022.
- Pittorino, F., Ferraro, A., Perugini, G., Feinauer, C., Baldassi, C., and Zecchina, R. Deep networks on toroids: removing symmetries reveals the structure of flat regions in the landscape geometry. In *International Conference on Machine Learning*, pp. 17759–17781. PMLR, 2022.
- Simonyan, K. and Zisserman, A. Very deep convolutional networks for large-scale image recognition. *arXiv preprint arXiv:1409.1556*, 2014.
- Singh, S. P. and Alistarh, D. Woodfisher: Efficient second-order approximation for neural network compression. *Advances in Neural Information Processing Systems*, 33: 18098–18109, 2020.
- Singh, S. P. and Jaggi, M. Model fusion via optimal transport. *Advances in Neural Information Processing Systems*, 33:22045–22055, 2020.
- Tatro, N., Chen, P.-Y., Das, P., Melnyk, I., Sattigeri, P., and Lai, R. Optimizing mode connectivity via neuron alignment. *Advances in Neural Information Processing Systems*, 33:15300–15311, 2020.
- Vaswani, A., Shazeer, N., Parmar, N., Uszkoreit, J., Jones, L., Gomez, A. N., Kaiser, Ł., and Polosukhin, I. Attention is all you need. *Advances in neural information processing systems*, 30, 2017.

- Wang, X., Wang, A. N., Zhou, M., and Ge, R. Plateau in monotonic linear interpolation—a” biased” view of loss landscape for deep networks. *arXiv preprint arXiv:2210.01019*, 2022.
- Wortsman, M., Horton, M. C., Guestrin, C., Farhadi, A., and Rastegari, M. Learning neural network subspaces. In *International Conference on Machine Learning*, pp. 11217–11227. PMLR, 2021.
- Wortsman, M., Ilharco, G., Gadre, S. Y., Roelofs, R., Gontijo-Lopes, R., Morcos, A. S., Namkoong, H., Farhadi, A., Carmon, Y., Kornblith, S., et al. Model soups: averaging weights of multiple fine-tuned models improves accuracy without increasing inference time. In *International Conference on Machine Learning*, pp. 23965–23998. PMLR, 2022.
- Yamada, M., Yamashita, T., Yamaguchi, S., and Chijiwa, D. Revisiting permutation symmetry for merging models between different datasets. *arXiv preprint arXiv:2306.05641*, 2023.
- Ye, J., Lu, X., Lin, Z., and Wang, J. Z. Rethinking the smaller-norm-less-informative assumption in channel pruning of convolution layers. *arXiv preprint arXiv:1802.00124*, 2018.
- Yunis, D., Patel, K. K., Savarese, P. H. P., Vardi, G., Frankle, J., Walter, M., Livescu, K., and Maire, M. On convexity and linear mode connectivity in neural networks. In *OPT 2022: Optimization for Machine Learning (NeurIPS 2022 Workshop)*, 2022.
- Zhang, H., Dauphin, Y. N., and Ma, T. Fixup initialization: Residual learning without normalization. *arXiv preprint arXiv:1901.09321*, 2019.
- Zhou, Z., Yang, Y., Yang, X., Yan, J., and Hu, W. Going beyond linear mode connectivity: The layerwise linear feature connectivity. *arXiv preprint arXiv:2307.08286*, 2023.
- Zimmer, M., Spiegel, C., and Pokutta, S. Sparse model soups: A recipe for improved pruning via model averaging. *arXiv preprint arXiv:2306.16788*, 2023.

Appendix

The appendix includes complete results of experiments reported in the main paper and additional results and discussions that are unable to be presented in the main body due to space limits. The organization is as follows:

Appendix A. Discuss the limitations of this work and some future work.

Appendix B. Provide additional related work.

Appendix C. Provide complete experimental details of this work.

Appendix D. Supplementary to Sec. 2, including the comparison of different implementations of activation matching in Ainsworth et al. (2022), Jordan et al. (2022), and this work.

Appendix E. Supplementary to Sec. 3, including a successful example of multi-matching on MLP + MNIST, the discussion on the distance between models before/after matching, and more experimental results.

Appendix F. Supplementary to Sec. 4, including more discussions on REPAIR and RESCALE, a novel data-independent re-normalization variant, experiments on the Fisher Information, and additional results demonstrating the benefit brought by the implicit bias of large learning rate and large weight decay.

Appendix G. Supplementary to Sec. 5, including additional pruning results on various model architectures and datasets and further discussions.

A. Limitation and Future Work

- As one of the first comprehensive studies towards understanding previous successes and failures in model re-basin, this work only focuses on the fundamental setup — re-basing models trained on the same dataset and the most studied model architectures and datasets in prior works to remove unnecessary difficulties and concentrate on the intrinsic principle. We leave the consideration of more networks (e.g., transformer-based models as studied in Imfeld et al. (2023)) and datasets for future work.
- Our analysis in Sec. 4.2 and 4.3 partly draws upon the perspective from many previous studies (Han et al., 2015; Li et al., 2016) that the magnitude of one parameter in a trained model can, to some extent, represent its significance and the amount of information stored there. Although this view might not be universally correct, especially in the context of structural pruning (Ye et al., 2018), we emphasize that our extensive experimental results well support the entire logic presented in this paper and, most importantly, lead to novel findings (Sec. 4.3 and 5) that are not mentioned in any prior work, to our best knowledge. With a main focus on improving the practice, it’s expected that more results could be derived from there, and we leave this for future work. Meanwhile, we also provide results on the Fisher Information in Appendix F.
- Sec. 4.3 reveals that the implicit bias of the training with a large learning rate and weight decay is beneficial to re-basin. Yet, we observed that the improvement degraded once the learning rate and weight decay were set too large. While this seems to restrict the empirical value of our finding, it’s noteworthy that this connection indeed indicates that any existing and coming understanding of the effect of learning rate and weight decay could enhance our understanding of model re-basin and potentially improve the standard practice. With the extensive prior work on learning rate (Mohtashami et al., 2023; Andriushchenko et al., 2023b) and weight decay (Andriushchenko et al., 2023a), we expect to make the most of this connection and leave this for future work. The same statement applies to the connection between pruning and re-basin and linear mode connectivity presented in Sec. 4.2.
- With the main focus on model re-basin and the linear mode connectivity, we only demonstrate the power of re-normalization in pruning in the one-shot pruning scenario, but we emphasize that the same logic applies to other pruning frameworks, e.g., structured pruning and gradual pruning. We regard this as a promising direction worthy of further exploration and leave this as our future work. This super lightweight yet powerful technique is especially believed to be valuable in resource-limited deep learning. Meanwhile, we only consider a simple hyperparameter setting for the advanced WoodFisher pruner, i.e., fisher subsample size = 80 and fisher mini-batch size = 100 for ImageNet pruning, to save computational cost. Although this restricts the ability of the pruner, a significant improvement by REPAIR/RESET is already demonstrated in our results and should be universal after merely changing some hyperparameters. We leave the efforts towards improving the SOTA results for future work.

- We reveal an intriguing observation that removing biases from the plain model can significantly reduce the barrier in the same way as re-normalization. This observation is also connected to the results shown in Wang et al. (2022). We expect that a deeper understanding of this could potentially provide more insights on how to improve the matching or post-matching process. We leave this for future work.

B. More Related Work

Early works (Draxler et al., 2018; Garipov et al., 2018) conjectured and empirically verified that the different neural network loss minima could indeed be connected by simple curves along which the loss remains low — a phenomenon called *Mode Connectivity*. Freeman & Bruna (2016) provided an asymptotical proof on half-rectified single-layer networks. Gotmare et al. (2018) empirically validated the claim in extreme cases where the input models were trained or initialized differently. Taturo et al. (2020) proposed a neuron alignment algorithm that seeks permutations between trained networks, after which it is easier to learn a simple, planar, low-loss curve efficiently. Wortsman et al. (2021); Benton et al. (2021) directly learned lines, curves, and simplexes, preserving the mode connectivity. Generally, the mode connectivity can also be utilized as a powerful tool to analyze, e.g., the loss landscape (Gotmare et al., 2018) and the model’s mechanisms (Lubana et al., 2023).

Regarding the linear case, the LMC was first observed to exist between solutions trained from the same initialization. The shared initialization can either be a checkpoint in early training (Nagarajan & Kolter, 2019; Frankle et al., 2020) or a pre-trained network served as the starting point in transfer learning (Neyshabur et al., 2020). Empirical observations (Neyshabur et al., 2020; Fort et al., 2020) suggested that these models were trained into the same basin on the loss landscape, and averaging them could produce a better-performed model and save the additional storage and computational cost compared to model ensemble (Wortsman et al., 2022; Zimmer et al., 2023; Izmailov et al., 2018; Juneja et al., 2022). The latter improvement is reasonable, assuming the basin is nearly convex, and hence, the average model is closer to the center of the basin. One empirical support for this intuition was demonstrated in Yunis et al. (2022), where the authors found a high-dimensional convex hull of low loss between the endpoints of several SGD trajectories. The LMC was also found to have connections to a wide range of fields, including the Lottery Ticket Hypothesis (Frankle et al., 2020; Frankle & Carbin, 2018; Paul et al., 2022) and the neural tangent kernel (NTK) (Fort et al., 2020). In the context of transfer learning, Juneja et al. (2022) found that the fine-tuned models could be divided into distinct clusters where LMC only existed between models within the same cluster. Model averaging/merging is also found to be highly helpful on the large language models (Ilharco et al., 2022).

On the other hand, a substantial linear barrier was often observed (Neyshabur et al., 2020; Frankle et al., 2020) between independent SGD solutions, which restricts the application of model averaging. Entezari et al. (2021) compared models trained from different initializations and conjectured that the barrier could be eliminated after accounting for the permutation invariance of neural networks, assuming the model is wide enough. The claim was proved for a wide enough fully connected network with a single hidden layer at initialization. Although the paper failed to empirically validate this conjecture by finding desired permutations to re-basin the model, a successful attempt was shown in (Ainsworth et al., 2022), where three different matching algorithms were derived for this purpose. Notably, these algorithms succeeded in obtaining the zero-barrier LMC between independently trained ResNet models on CIFAR-10 for the first time. Prior and concurrent work in this direction includes Benzing et al. (2022) proposing a matching algorithm to align models at initialization and Singh & Jaggi (2020) deriving a powerful optimal-transport-based algorithm. The latter work focused on the soft alignment (a.k.a., model fusion) between models and is hence not particularly considered in our work. Recent work in this direction is Imfeld et al. (2023) providing efforts to fuse transformers (Vaswani et al., 2017). It’s also noteworthy that the matching algorithms proposed in many works have some common points, e.g., the activation matching algorithm in Ainsworth et al. (2022) and Singh & Jaggi (2020) and the matching algorithm in Taturo et al. (2020). While a significant improvement was seen in Ainsworth et al. (2022), Jordan et al. (2022) emphasized that this success highly depended on the utilization of normalization layers in models, including BatchNorm (with RESET) and LayerNorm, and the matching algorithms performed poorly on plain models without normalization layers. The authors attributed this to the issue of “variance collapse” and addressed it by proposing REPAIR — an extension of RESET that could work on plain models. Despite the extensive empirical studies, the understanding of this field remains limited. A theoretical effort was recently provided in Ferbach et al. (2023), which proved the LMC via model re-basin in the mean field regime and generalized the results to deep networks under some assumptions.

Besides the original re-basin practices between two models trained on the same dataset, Yamada et al. (2023); Ainsworth et al. (2022); Jordan et al. (2022) explored aligning models trained on different datasets, and a preliminary result on matching multiple MLPs trained on MNIST was reported in Ainsworth et al. (2022). Recently, Adilova et al. (2023) and Zhou et al. (2023) studied the *Layerwise Linear Mode Connectivity*. Pittorino et al. (2022) utilized the re-basin approaches to remove

symmetry and revealed the structure of flat regions in the loss landscape. Different from the standard re-basin practice, it also considered the scaling invariance.

C. Experimental Detail

We present all experimental details in this section.

Training Setting. The fundamental training framework is based on the standard setup [Frankle et al. \(2020\)](#); [He et al. \(2016\)](#). We train the model with standard SGD (momentum = 0.9) with a batch size of 128. For standard complete training of VGG and ResNet on CIFAR-10 and CIFAR-100, the model is trained for 160 epochs with a step decay learning rate initialized at 0.1 and reduced by a factor of 10 at iteration 32,000 and 48,000 (\sim epoch 82 and 123). Weight decay is set as $wd = 10^{-4}$. For the learning rate comparison experiment in [Sec. 4.3](#), the initial learning rate is selected from [0.01, 0.03, 0.05, 0.07, 0.1]. For the weight decay experiment, the weight decay factor is selected from $[10^{-4}, 2 \times 10^{-4}, 3 \times 10^{-4}, 4 \times 10^{-4}, 5 \times 10^{-4}]$.

For smooth training, we perform some modifications to the training settings of certain models. There are two different learning rate schedules for this. For training VGG16 with $wd > 10^{-4}$, VGG16 ($8 \times$ width), ResNet20 ($4 \times$ width), and ResNet20 LN, the learning rate linearly increases in the first epoch from 10^{-6} to 0.1 and then follows the same step decay schedule. For training VGG16 without biases, plain ResNet20/ResNet32 (with and without biases), and Fixup ResNet20, the learning rate experiences the same linear warm-up in the first epoch but then follows a cosine annealing schedule. For training VGG16 LN with Kaiming uniform initialization, both learning schedules work well, and most of the results (e.g., when comparing different initializations in [Sec. 4.3](#)) reported in the paper are based on the step decay schedule with a linear warm-up. The same linear warm-up + cosine annealing schedule is applied when training VGG11 on CIFAR-100, but the warm-up takes two epochs. In our experiments, we didn’t observe differences brought by the learning rate schedule, and those modifications were just for robust training.

For the retraining experiment in [Sec. 3.2](#), one pre-trained network is firstly pretrained using SGD (momentum= 0.9, lr = 0.1, $wd = 10^{-4}$) for 20 epochs to move outside the basin and is then trained with a small lr = 0.01 for another 5 epochs to return to the basin but land at a different place. In [Sec. 3.4](#), after removing biases, models are trained for another 10 epochs with the lr= 0.01 and momentum= 0.9, without the weight decay. For the retraining experiment in [Sec. 4.2](#), a small learning rate lr = 0.01 is utilized and wd is set to $1e - 4$. We set a maximal training epoch of 15 or 20 (which can be inferred from the x-axis in the plot) if the training accuracy of the model doesn’t achieve 90% within the given budget.

For training VGG16 LN on MNIST reported in [Sec. 4.3](#), we replicated the training setting of [Ainsworth et al. \(2022\)](#). The model is initialized with Kaiming uniform initialization and trained for 25 epochs with SGD (momentum = 0.9). The learning rate linearly increases within the first epoch until reaching the maximum 0.001/0.01/0.1 and then follows a cosine annealing schedule. The training batch size is 100. Weight decay is set as $wd = 5 \times 10^{-4}$.

Model Architecture. The MLP used in our experiments consists of two hidden layers of width 120 and 84 with ReLU activation. The basic architectures of VGG and ResNet for CIFAR-10 and CIFAR-100 follow [Frankle et al. \(2020\)](#) and are standard in relevant practices. We edit the normalization layers accordingly in the plain/BN/LN version. For plain ResNet, we also consider the one with biases in convolutional layers. The code for Fixup ResNet is adapted from the original paper ([Zhang et al., 2019](#)). For pruning ResNet50 on ImageNet, we directly utilized the pre-trained network in Torchvision ([Marcel & Rodriguez, 2010](#)).

D. Supplementary to Sec. 2

D.1. Practical Calculation of Barrier

In our experiments, it was observed that the maximal barrier was almost surely achieved at the middle (i.e., $\lambda = 0.5$), and hence we simply set $\lambda = 0.5$ ([Def. 2.1](#)) when measuring the barrier to save computational cost. This empirical measurement is also adopted in ([Entezari et al., 2021](#)). For all the interpolation plots reported in the paper, we uniformly select 11 interpolation points between the two end models.

D.2. Different Implementations of Activation Matching

We noticed that although [Jordan et al. \(2022\)](#) and [Ainsworth et al. \(2022\)](#) utilized the same activation matching algorithm, their implementations are different and the results can differ much. For convenience, we will refer to the implementation

Table 2. Compare different implementations of activation matching. Running on NVIDIA RTX A5500 (24G). The best results in each line are in bold.

Model	Barrier (Test Accuracy)			Running Time		
	Ours	A	B	Ours	A	B
VGG16	37.52 \pm 5.76%	54.87 \pm 5.12%	37.53 \pm 5.78%	17.87 \pm 0.29 s	7.75 \pm 0.09 s	40.91 \pm 0.35 s
VGG16 BN	3.51 \pm 0.15%	4.33 \pm 0.29%	3.49 \pm 0.13%	17.97 \pm 0.28 s	8.84 \pm 0.11 s	45.14 \pm 0.38 s
VGG16 LN	6.9 \pm 0.8%	9.71 \pm 0.66%	-	20.14 \pm 0.37 s	11.48 \pm 0.15 s	-
ResNet20	29.49 \pm 3.76%	32.45 \pm 2.15%	-	5.66 \pm 0.03 s	5.41 s	-
ResNet20 LN	23.05 \pm 1.84%	24.58 \pm 3.26%	-	8.21 \pm 0.09 s	9.12 \pm 0.18 s	-

used in Ainsworth et al. (2022) as **A** and the one used in Jordan et al. (2022) as **B**. Both implementation **A** and **B** first estimate the activation statistics (mean and std.) of each layer in an online way and then solve the linear assignment problem based on the Pearson correlation calculated from the activation statistics. The main issue occurs in the former process, consisting of two parts: (1) implementation **A** utilizes the default `Float` data type, while **B** adopts a more accurate `Double` type; (2) to calculate the average covariance, implementation **A** first accumulates the summation by feeding the entire dataset to the model and then takes the average; while **B** calculates each batch average and then takes the average of batch averages. This results in a generally worse performance of implementation **A**.

Since this work aims to delve deeper into the SOTA practice and improve from there, we adopted the calculation strategy in **B**. We also noticed that although implementation **B** normally owned a better performance, it ran extremely slowly. The reason is that it performs the matching sequentially, i.e., re-feeding all the data to the model when matching each pair of layers; while **A** only feeds data in a single run and accumulates all the statistics simultaneously. In our experiments, we didn’t find an obvious difference between them in performance. Therefore, our approach is mainly based on implementation **A** but utilizes the statistics accumulation strategy in **B**. We report the results on matching models trained on CIFAR-10 in Table 2. We compare the three implementations on plain VGG16 and VGG16 BN and compare our approach with implementation **A** in other settings. The results demonstrate that our approach has the best trade-off between high performance and computational efficiency.

E. Supplementary to Sec. 3

E.1. Plain Matching

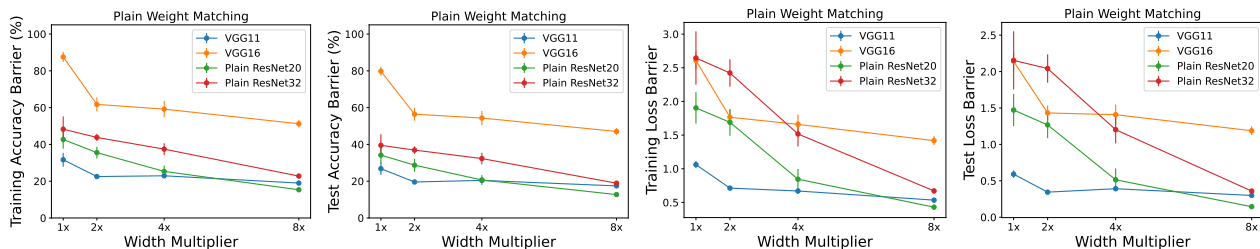


Figure 7. Barrier between independent plain models trained on CIFAR-10. Weight matching is applied.

We report the complete plain weight matching results in Figure 7. In addition, the results of plain activation matching are also shown in Figure 8. Generally, the barrier decreases as the model width gets larger. The only exception is plain activation matching on VGG11 and VGG16. The standard deviation in the plots also suggests that the performance of matching becomes more stable between wider models. We emphasize that although the results partly support the existence of LMC through permutation between sufficiently wide models as conjectured in prior works (Ainsworth et al., 2022; Entezari et al., 2021), the barrier reduction rate observed in our results was too small to have a practical impact due to the storage and computational constraints.

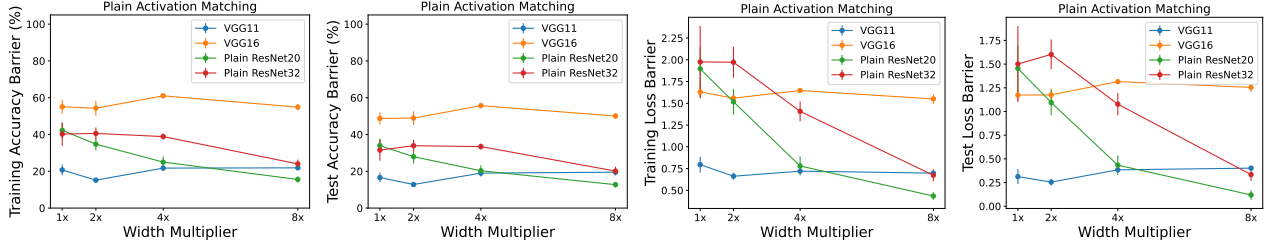


Figure 8. Barrier between independent plain models trained on CIFAR-10. Activation matching is applied.

E.2. Comparison with Same Basin Scenario

The complete results are illustrated in Figure 9, 10, 11 and 12, including additional results of ResNet20 (4x width) + CIFAR-10. In all settings, a RESET was not found necessary when averaging models in the same basin. Figure 10 and 12 suggest that the current matching algorithms can already recover the basin after a random permutation. Notably, it almost surely identified the exact permutation applied to the basin in our experiments. We present the retraining dynamics in Figure 13. Especially, we recorded the L_2 distance (including BN statistics) between the new model and the original solution to validate that this process indeed returned a different solution but close to the prior one.

In our experiments, we also noticed that the distance between independent models didn't decrease too much after matching. We report the results of various models trained on CIFAR-10 in Table 3. We conjecture this is another piece of evidence that current matching practices fail to truly re-basin independent solutions. This type of distance analysis was also shown in (Neyshabur et al., 2020).

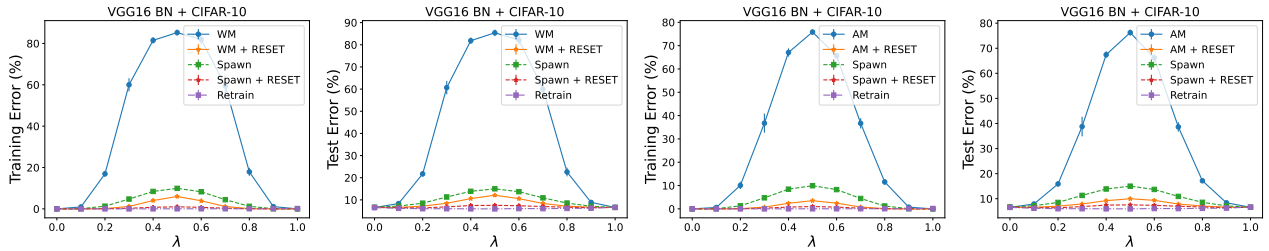


Figure 9. Comparison between re-basin and the same basin scenario. Linear interpolation between two VGG16 BN trained on CIFAR-10 is illustrated.

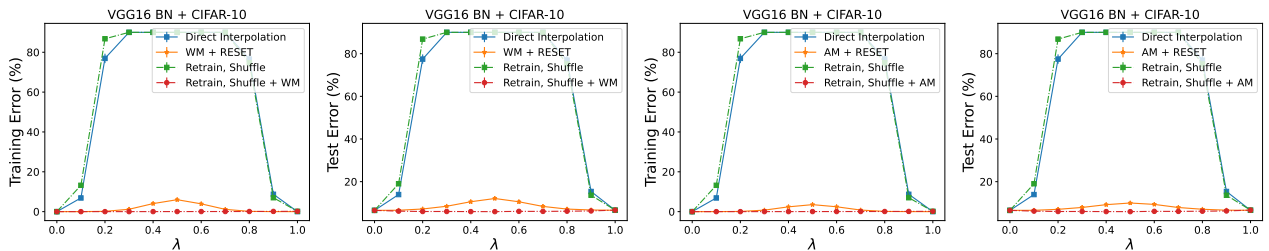


Figure 10. Comparison between re-basin and the same basin scenario. Linear interpolation between two VGG16 BN on CIFAR-10 is illustrated.

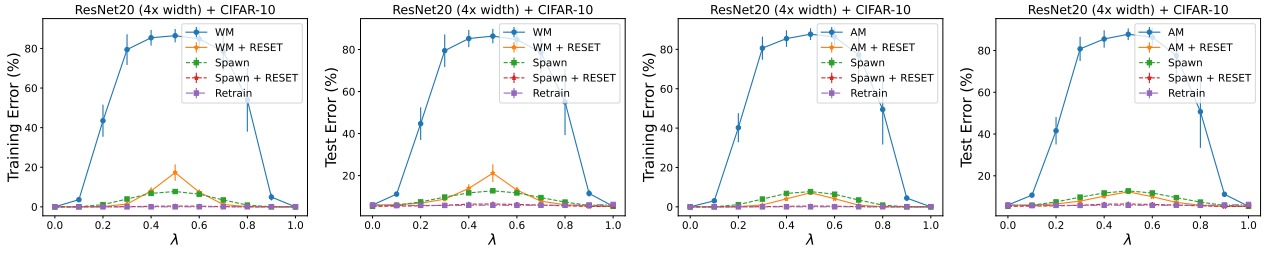


Figure 11. Comparison between re-basin and the same basin scenario. Linear interpolation between two ResNet20 (4× width) trained on CIFAR-10 is illustrated.

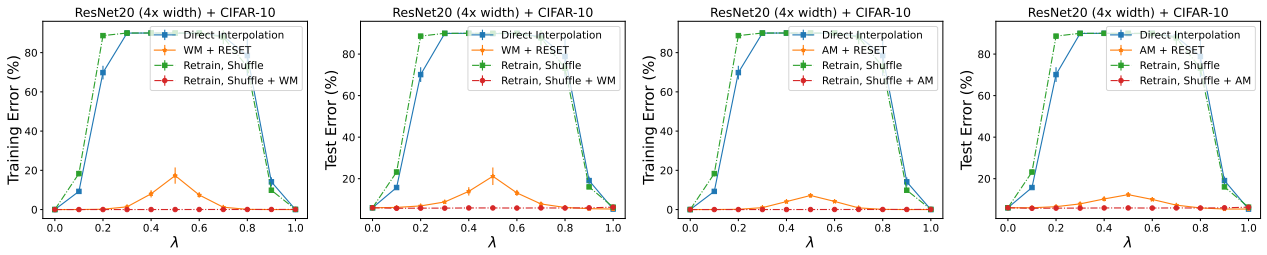


Figure 12. Comparison between re-basin and the same basin scenario. Linear interpolation between two ResNet20 (4× width) on CIFAR-10 is illustrated.

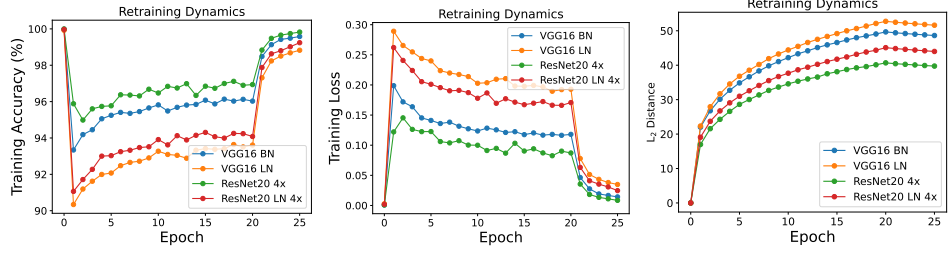


Figure 13. Retraining dynamics. “4x” refers to 4× width models.

Table 3. Compare the L_2 distance before/after matching. Results with * exclude the BatchNorm statistics.

Model	Original	WM	AM
VGG16 BN	100.32 ± 0.59	84.5 ± 0.25	88.26 ± 0.47
VGG16 LN	101.13 ± 0.04	89.65 ± 0.06	91.81 ± 0.1
ResNet20 (4× width)	99.22 ± 0.3	84.58 ± 2.61	91.69 ± 1.99
ResNet20 LN (4× width)	91.69 ± 0.18	79.62 ± 0.28	82.28 ± 0.16
VGG16 BN*	91.31 ± 0.24	83 ± 0.24	83.97 ± 0.21
ResNet20 (4× width)*	81.83 ± 0.01	76.69 ± 0.55	77.66 ± 0.39

E.3. Multiple Model Matching

We present the algorithmic details of the three multiple-matching algorithms in Algorithms 1, 2, and 3. The iterative matching is extremely time-consuming and often could not converge in a limited time (given several hours in our experiments). Consequently, we manually terminated the algorithm if it had run 30 iterations, which might be the reason for its unstable performance in our experiments.

Algorithm 1 Reference Matching

Input: Model parameters $\theta_1, \theta_2, \dots, \theta_n$

Output: Merged model parameters $\bar{\theta}$

```

1:  $\tilde{\theta}_1 \leftarrow \theta_1$ 
2: for  $i = 2, \dots, n$  do
3:    $\pi_i \leftarrow \text{MatchingAlgorithm}(\theta_1, \theta_i)$ 
4:    $\tilde{\theta}_i \leftarrow \pi_i(\theta_i)$ 
5: end for
6:  $\bar{\theta} = \frac{\sum_{i=1}^n \tilde{\theta}_i}{n}$ 
    
```

Algorithm 2 Sequential Matching

Input: Model parameters $\theta_1, \theta_2, \dots, \theta_n$

Output: Merged model parameters $\bar{\theta}$

```

1:  $\tilde{\theta}_1 \leftarrow \theta_1$ 
2: for  $i = 2, \dots, n$  do
3:    $\pi_i \leftarrow \text{MatchingAlgorithm}(\tilde{\theta}_{i-1}, \theta_i)$ 
4:    $\tilde{\theta}_i \leftarrow \pi_i(\theta_i)$ 
5: end for
6:  $\bar{\theta} = \frac{\sum_{i=1}^n \tilde{\theta}_i}{n}$ 
    
```

Algorithm 3 Iterative Matching

Input: Model parameters $\theta_1, \theta_2, \dots, \theta_n$

Output: Merged model parameters $\bar{\theta}$

```

1:  $\tilde{\theta}_i \leftarrow \theta_i, i = 1, \dots, n$ 
2: repeat
3:   for  $i \in \text{RandomPermutation}(1, \dots, n)$  do
4:      $\tilde{\theta}_{\text{ref}} = \frac{\sum_{j \neq i} \tilde{\theta}_j}{n-1}$ 
5:      $\pi_i \leftarrow \text{MatchingAlgorithm}(\tilde{\theta}_{\text{ref}}, \tilde{\theta}_i)$ 
6:      $\tilde{\theta}_i \leftarrow \pi_i(\tilde{\theta}_i)$ 
7:   end for
8: until Convergence
9:  $\bar{\theta} = \frac{\sum_{i=1}^n \tilde{\theta}_i}{n}$ 
    
```

The complete results are visualized in Figure 14 and 15. In all settings, the performances of all algorithms rapidly degraded as we increased the number of models to be merged. In comparison, we also showcase one scenario where the same practices can successfully match independent solutions, as shown in Figure 16. There, we considered matching 8 MLPs trained on MNIST. This setting was also considered in Ainsworth et al. (2022) through the iterative matching, while here we show that a simple reference matching or sequential matching already suffices.

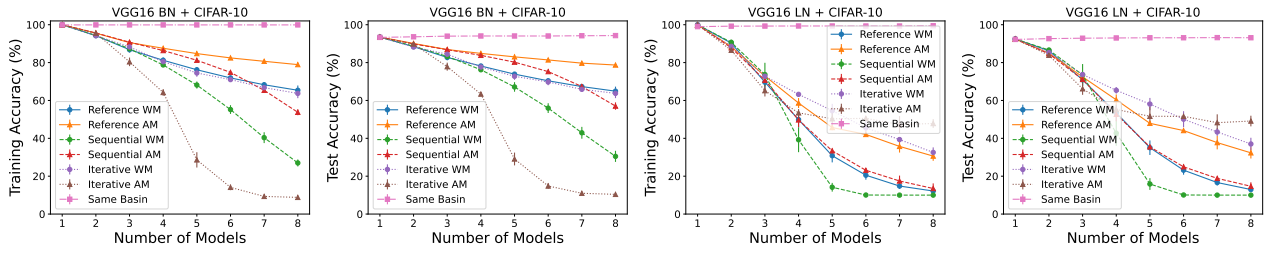


Figure 14. Accuracy of the average model in multiple matching. **Left:** VGG16 BN + CIFAR-10. **Right:** VGG16 LN + CIFAR-10.

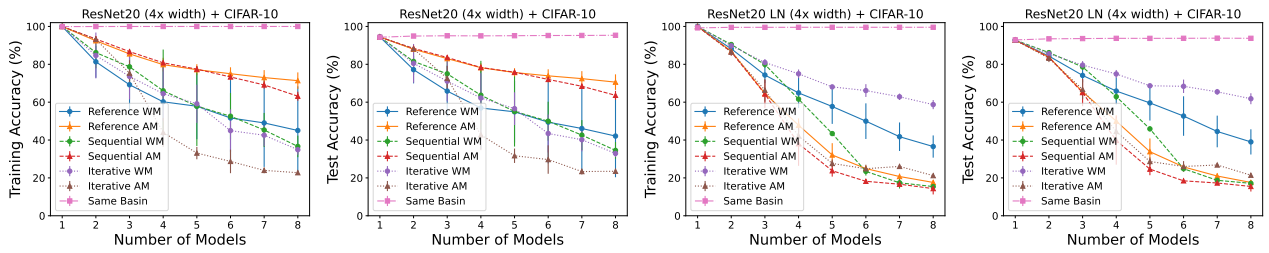


Figure 15. Accuracy of the average model in multiple matching. **Left:** ResNet20 (4x width) + CIFAR-10. **Right:** ResNet20 LN (4x width) + CIFAR-10.

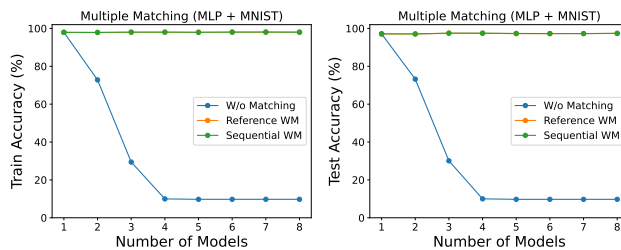


Figure 16. Accuracy of the average model in multiple matching. MLP + MNIST.

E.4. Remove Biases and Re-Normalization

We present the complete results of removing bias in Figures 17, 18, 19, 20, 21, 22, 23 and 24. The improvement brought by removing bias consistently holds among all the settings we considered, including VGG16/plain ResNet20 + CIFAR-10 and VGG11/plain ResNet20 + CIFAR-100. The finding is also motivated by the small barrier achieved on no-bias plain models in (Singh & Jaggi, 2020).

It was also observed that this improvement was similar to that brought by re-normalization. Specifically, we compared it with RESCALE on VGG16 + CIFAR-10 and with REPAIR on plain ResNet20 + CIFAR-10, shown in Figure 25 and 26, respectively. We suspect that understanding this intriguing analogy could potentially provide more insights on how to improve the matching or post-matching process. For instance, one interesting question is what is the common issue alleviated by both strategies. If there is one such factor, it's possible to further improve the SOTA by directly optimizing that. We leave this for future work.

We also drew another interesting observation. We noticed that, although the post-matching linear barrier on the accuracy landscape significantly decreased after removing biases from the model, the barrier on the loss landscape remained, as shown in Figures 17, 18, 19, 20, 21, 22, 23 and 24. A similar observation was drawn by Wang et al. (2022) where the homogeneous interpolation can only change the linear interpolation shape on the accuracy landscape. We regard this as one of the challenges for understanding why removing biases can improve performance and leave this for future work.

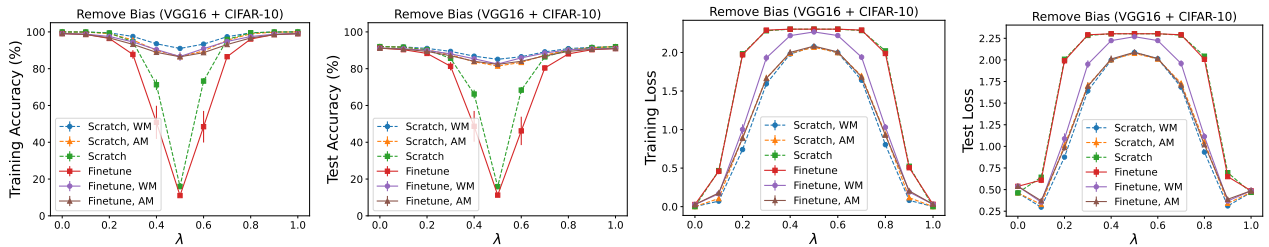


Figure 17. Training from scratch without biases vs. removing biases in a pre-trained model followed by fine-tuning. Linear interpolation between two VGG16 on CIFAR-10 is illustrated.

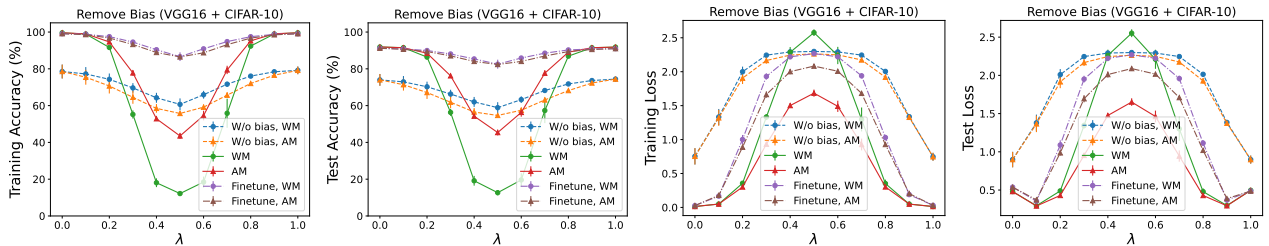


Figure 18. Removing biases in a pre-trained model followed by fine-tuning. Linear interpolation between two VGG16 on CIFAR-10 is illustrated.

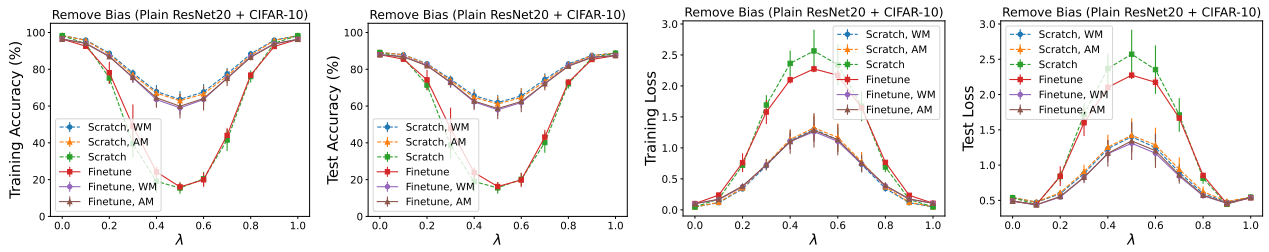


Figure 19. Training from scratch without biases vs. removing biases in a pre-trained model followed by fine-tuning. Linear interpolation between two plain ResNet20 on CIFAR-10 is illustrated.

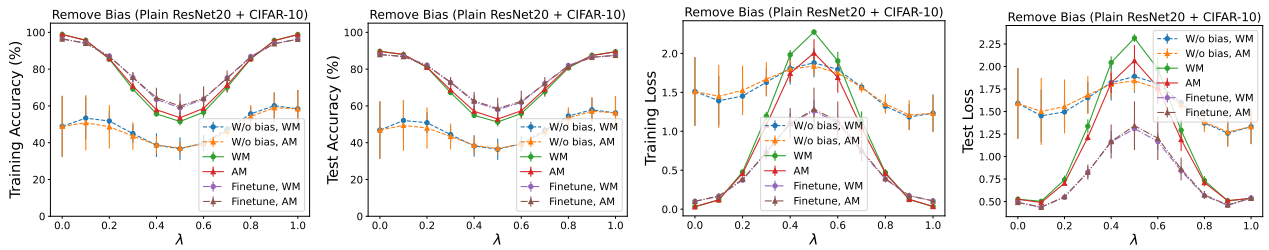


Figure 20. Removing biases in a pre-trained model followed by fine-tuning. Linear interpolation between two plain ResNet20 on CIFAR-10 is illustrated.

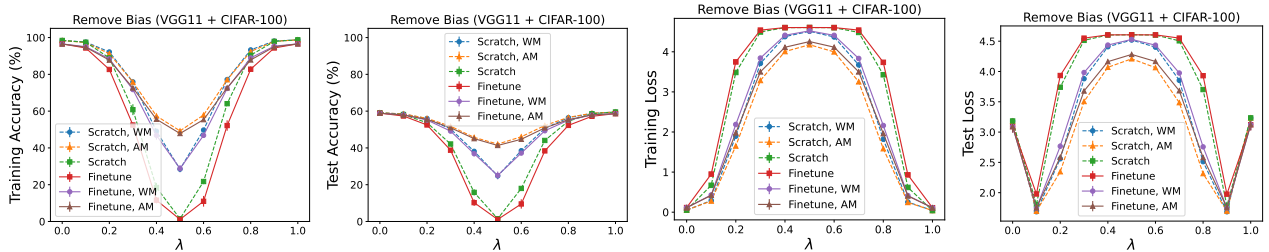


Figure 21. Training from scratch without biases vs. removing biases in a pre-trained model followed by fine-tuning. Linear interpolation between two VGG11 on CIFAR-100 is illustrated.

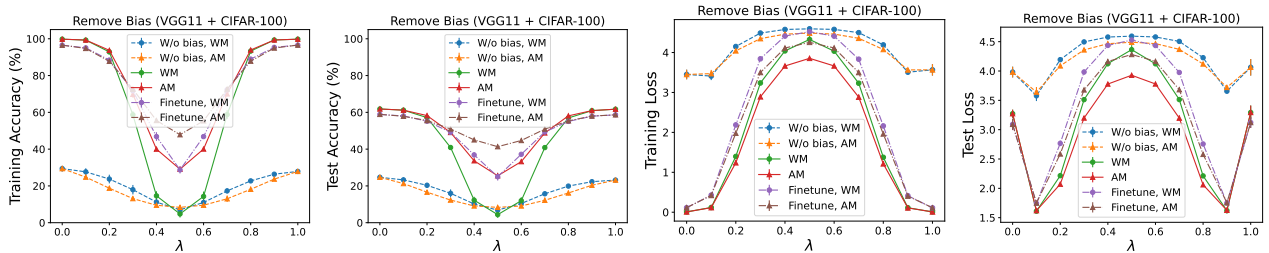


Figure 22. Removing biases in a pre-trained model followed by fine-tuning. Linear interpolation between two VGG11 on CIFAR-100 is illustrated.

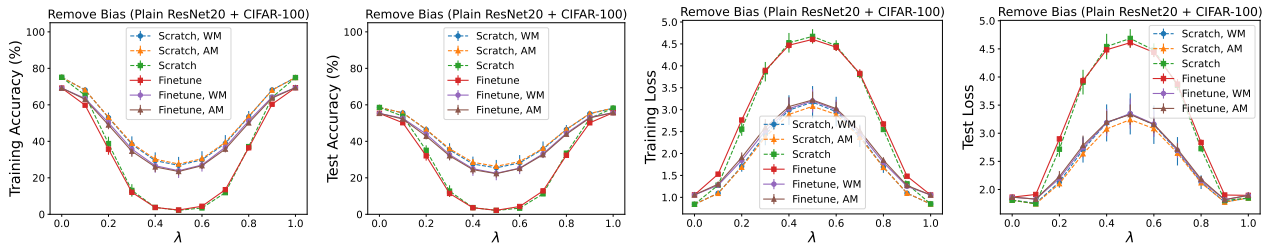


Figure 23. Training from scratch without biases vs. removing biases in a pre-trained model followed by fine-tuning. Linear interpolation between two plain ResNet20 on CIFAR-100 is illustrated.

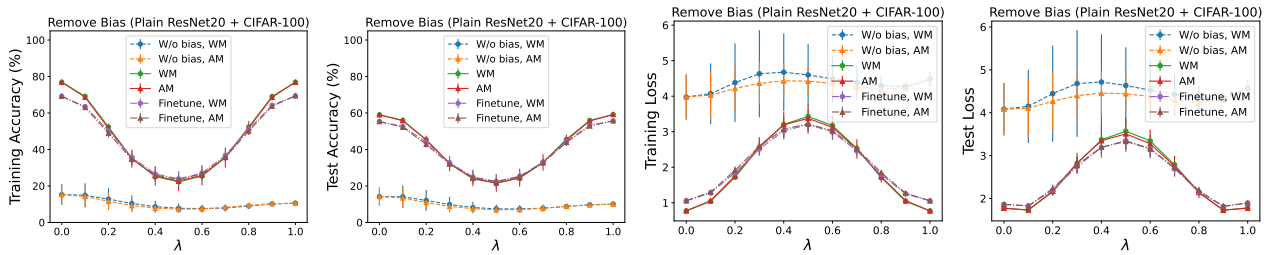


Figure 24. Removing biases in a pre-trained model followed by fine-tuning. Linear interpolation between two plain ResNet20 on CIFAR-100 is illustrated.

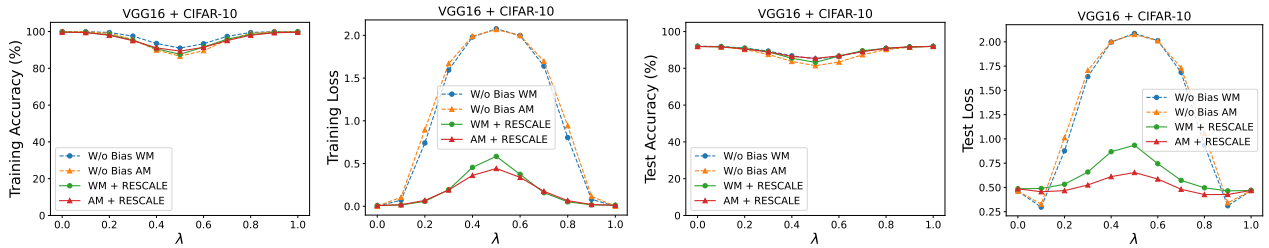


Figure 25. Removing biases vs. RESCALE. Linear interpolation between two VGG16 on CIFAR-10 is illustrated.

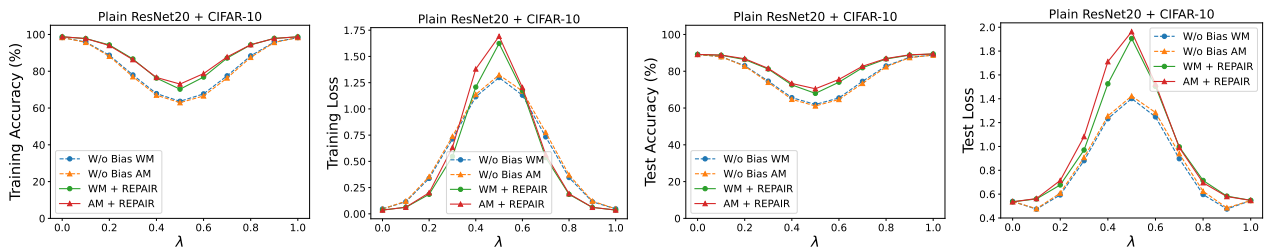


Figure 26. Removing biases vs. REPAIR. Linear interpolation between two plain ResNet20 on CIFAR-10 is illustrated.

E.5. Connection to Wang et al. (2022)

Wang et al. (2022) studies the monotonic linear interpolation (MLI) phenomenon: the loss and accuracy are typically monotonic on the line connecting a random initialization and the final SGD solution. This observation was previously regarded as evidence that the loss landscape around the SGD trajectory was nearly convex and hence the optimization was not too difficult (Goodfellow et al., 2014), while opposite observations were recently shown in Frankle (2020) where a long plateau often existed along this linear path on more advanced datasets. The results in Wang et al. (2022) suggest that the plateau on the linear path can be simply attributed to reasons such as the bias terms, the network initialization scale, and the network depth, which don't tell much about the difficulty of optimization. Under their assumptions, the authors proved that the biases and weights in the model play a different role in the linear interpolation and the results can be largely affected (e.g., become worse) by the biases. To demonstrate this, they proposed a *homogeneous interpolation* procedure when doing the interpolation (see Sec. 5 in (Wang et al., 2022)). This simple change in the calculation, surprisingly, removed the plateau and recovered the MLI.

We also tried this homogeneous interpolation in our experiments. As illustrated in Figures 27 and 28, we found this process also reduced the barrier. This observation suggested that the biases also play a significant role (at least for plain models) in linear interpolation between two independent solutions after matching. One analogy between the two scenarios is if we regard the poorly performed midpoint model as a model similar to the random initialization, the linear interpolation between two end models can be separated in the middle as the composition between two interpolations of the type “random init. – final solution”. Intriguingly, it was observed that the amount of barrier reduced by homogeneous interpolation was also similar to that bought by removing biases, and hence resembles that by re-normalization. As mentioned in the last section, another similarity is that homogeneous interpolation also can only affect the interpolation on the accuracy landscape. We believe these connections can shed light on a deeper understanding of the intrinsic principle under the hood, which is crucial for improving the practice.

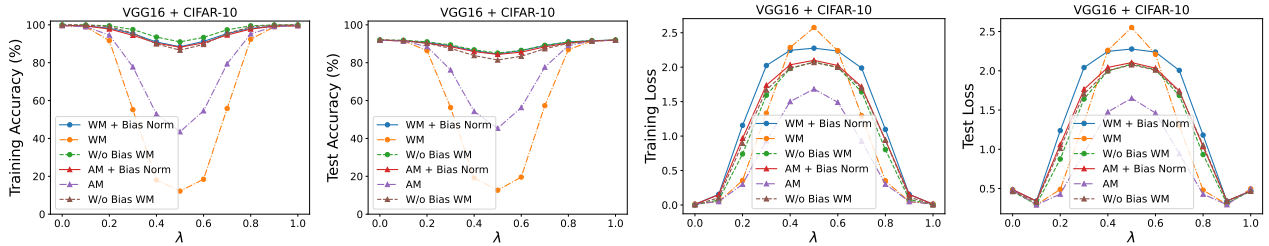


Figure 27. Linear interpolation between two VGG16 on CIFAR-10 is illustrated. The “Bias Norm” refers to the interpolation with Homogeneous normalization.

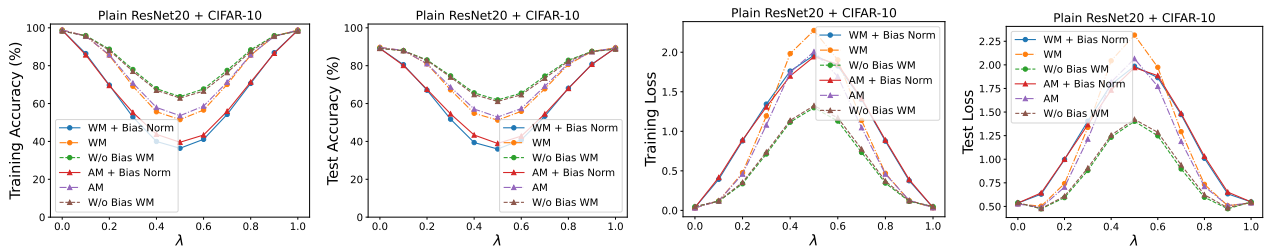


Figure 28. Linear interpolation between two plain ResNet20 on CIFAR-10 is illustrated. The “Bias Norm” refers to the interpolation with Homogeneous normalization.

F. Supplementary to Sec. 4

F.1. Effect of REPAIR: Rescaling

Full results of REPAIR ablation are present in Tables 4, 5, 6, 7, including VGG16, plain ResNet20 and Fixup ResNet20 trained on CIFAR-10 and VGG11 trained on CIFAR-100. Additionally, we observed that the goal statistics used in RESCALE can be selected even from an independent solution. We report one result in Table 8. There, the independent RESCALE still brings a significant improvement to the interpolated model for both matching algorithms. This finding further supports our claim that the key to REPAIR is to bring the scale of the activation back to the standard level.

Full activation statistics results are illustrated in Figures 29, 30, 32 and 33, including VGG16 and plain ResNet20 trained on CIFAR-10. In our experiments, we also noticed that the hidden activation statistics in the original midpoint model were similar to those in a randomly initialized model, shown in Figures 31 and 34. This indicates that without matching, the interpolated model loses the knowledge and degrades as a random model.

In Jordan et al. (2022), the aim of deriving REPAIR is to correct the statistics of hidden units in the interpolated network, including the running mean and running variance. In our experiments, we noticed that a more accurate calculation in this process could further improve the performance. In the original implementation, after setting the goal statistics in the interpolated model, REPAIR simultaneously accumulates the running statistics in each layer in a single run. However, the output of one layer is affected by early layers and hence a sequential calculation should return more accurate results. We verified this claim on VGG16 + CIFAR-10 with weight matching. As shown in Table 9, the sequential REPAIR outperforms the vanilla one by 8%, while no obvious differences were seen between RESCALE and sequential RESCALE. We argue that this result also suggests that the complete failure of RESHIFT is not trivial, as more accurate running means boosted by RESHIFT would also potentially improve the performance.

Table 4. Ablation study on REPAIR, VGG16 + CIFAR-10. The first line records the test accuracy of the original post-activation-matching midpoint model. The best result is in bold.

Variant	Test Accuracy
-	48.68 \pm 7.22 %
REPAIR	43.71 \pm 3.36 %
RESCALE	83.72 \pm 2.03 %
RESCALE (average)	75.97 \pm 2.78 %
RESHIFT	10 %

Table 5. Ablation study on REPAIR, VGG11 + CIFAR-100. The first line records the test accuracy of the original post-matching midpoint model. The best results in each column are in bold.

Variant	WM	AM
-	5.19 \pm 1.51 %	25.2 \pm 0.89 %
REPAIR	13.75 \pm 2.49 %	42.66 \pm 1.1 %
RESCALE	29.13 \pm 3.51 %	45.33 \pm 0.89 %
RESCALE (average)	18.19 \pm 2.44 %	34.06 \pm 0.86 %
RESHIFT	1 %	1 \pm 0.89 %

Table 6. Ablation study on REPAIR, Plain ResNet20 + CIFAR-10. The first line records the test accuracy of the original post-matching midpoint model. The best results in each column are in bold.

Variant	WM	AM
-	62.31 ± 5.43 %	61.42 ± 2.75 %
REPAIR	71.32 ± 3.33 %	72.22 ± 1.82 %
RESCALE	68.39 ± 4.82 %	72.01 ± 1.52 %
RESCALE (average)	61.05 ± 6.51 %	65.81 ± 3.18 %
RESHIFT	10.14 ± 0.25 %	10.12 ± 0.21 %

Table 7. Ablation study on REPAIR, Fixup ResNet20 + CIFAR-10. The first line records the test accuracy of the original post-matching midpoint model. The best results in each column are in bold.

Variant	WM	AM
-	38.84 ± 1.89 %	42.81 ± 0.23 %
REPAIR	63.62 ± 2.73 %	73.32 ± 0.15 %
RESCALE	61.85 ± 3.43 %	71.42 ± 0.23 %
RESCALE (average)	56.12 ± 2.41 %	67.26 ± 0.29 %
RESHIFT	10 %	10 %

Table 8. Ablation study on RESCALE, VGG16 + CIFAR-10. Results with * utilize the running statistics from an independent solution. The first line records the test accuracy of the original post-weight-matching midpoint model.

Variant	Test Accuracy
WM	10.49 %
WM + RESCALE*	68.89 %
WM + RESCALE (average)*	76.88 %
AM	43.98 %
AM + RESCALE*	68.64 %
AM + RESCALE (average)*	75.43 %

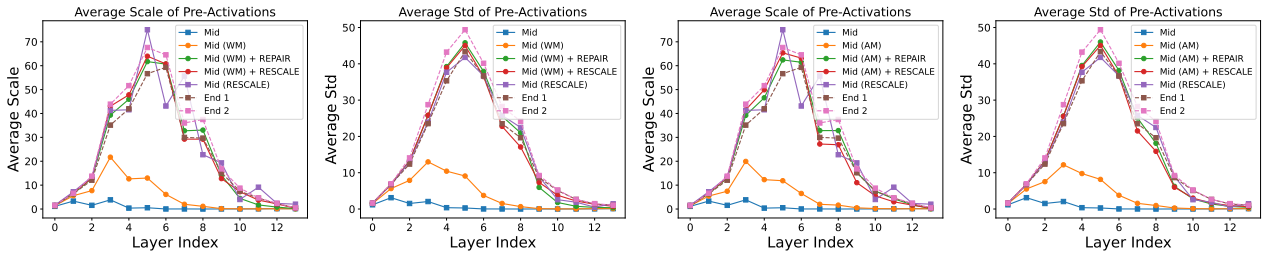


Figure 29. Pre-activation statistics of VGG16 trained on CIFAR-10, averaged in each layer.

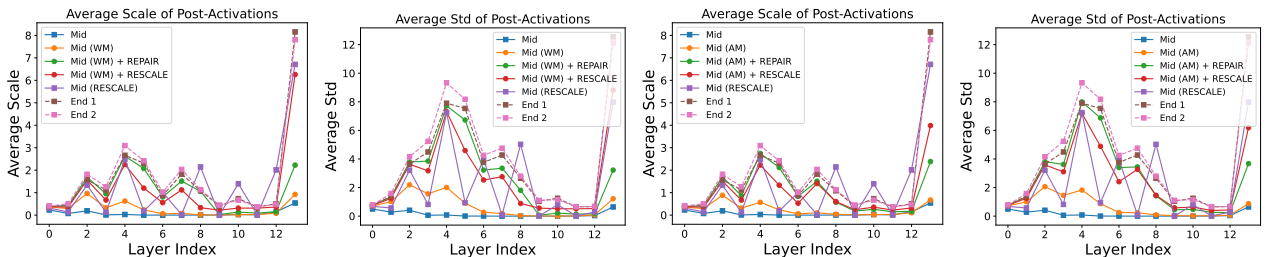


Figure 30. Post-activation statistics of VGG16 trained on CIFAR-10, averaged in each layer.

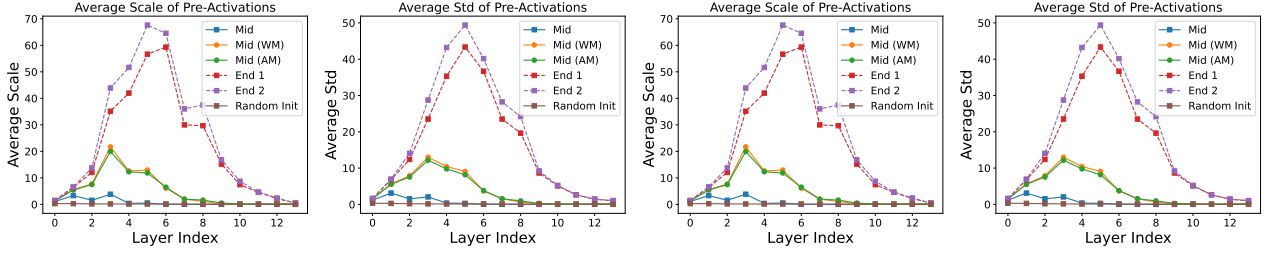


Figure 31. Pre-activation statistics of VGG16 trained on CIFAR-10, averaged in each layer. Compared with random initialization.

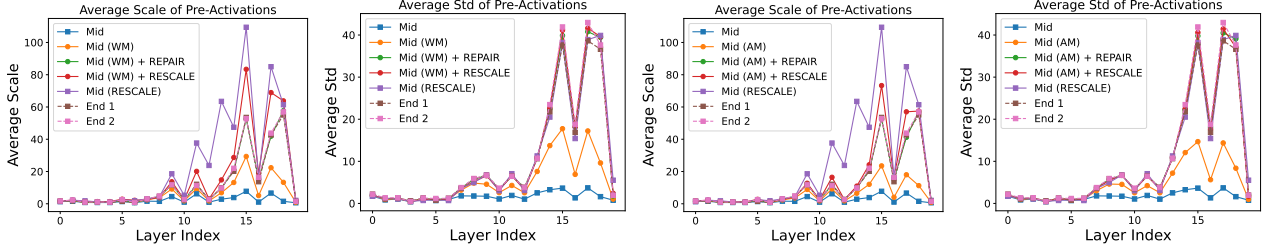


Figure 32. Pre-activation statistics of plain ResNet20 trained on CIFAR-10, averaged in each layer.

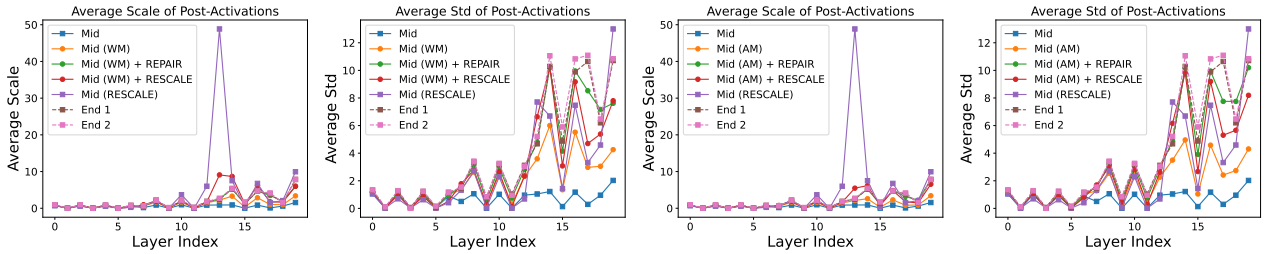


Figure 33. Post-activation statistics of plain ResNet20 trained on CIFAR-10, averaged in each layer.

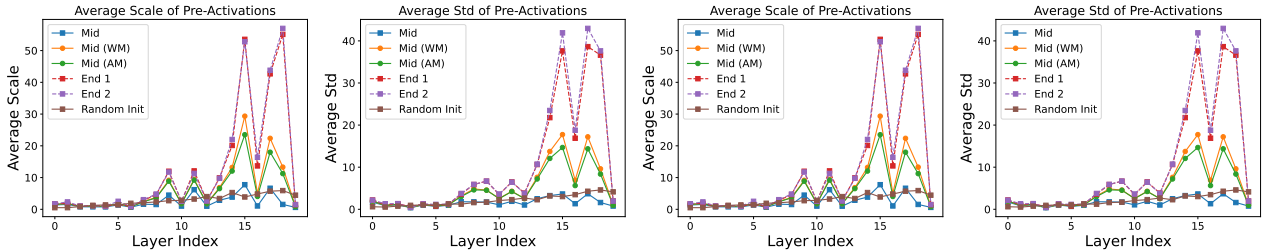


Figure 34. Pre-activation statistics of plain ResNet20 trained on CIFAR-10, averaged in each layer. Compared with random initialization.

Table 9. Compared with sequential re-normalization, evaluated on VGG16 + CIFAR-10. “SEQ” is short for “Sequential”. The best results in each column are in bold.

Variant	Train		Test	
	Acc	Loss	Acc	Loss
REPAIR	68.93%	1.59	65.75%	1.81
SEQ REPAIR	79.62%	1.33	75.38%	1.69
RESCALE	88.23%	0.59	83.63%	0.94
SEQ RESCALE	88.21%	0.59	83.57%	0.94

F.2. A Data-Independent Re-Normalization

In this section, we propose a novel data-independent re-normalization variant. It consists of two key points: (1) recording the running statistics of the end models during training, and (2) turning on the training mode in the interpolated model when evaluating. The first step is already satisfied for models with BatchNorm. For other models, it can be easily achieved by wrapping the layer in a customized module in which the running statistics are recorded during training. This modification removes the necessity of data when setting goal running mean and variance in the interpolated model. After setting the target statistics, rather than recording statistics in the interpolated model by feeding training data, the model is directly employed for evaluation, but in a training mode. This means that running statistics are automatically recorded during evaluation. We observed that this approach can achieve comparable performance to the vanilla method, as shown in Tables 10 and 11, while exhibiting a distinct advantage in terms of data independence. In addition, it was also found that several batches of data already sufficed when recording the statistics.

Table 10. Data-independent RESET, evaluated on VGG16 BN + CIFAR-10. The final test accuracy of the midpoint model is reported.

Variant	WM	AM
Original	88.74%	88.51%
Data Independent	86.59%	86.44%

Table 11. Data-independent REPAIR/RESCALE, evaluated on VGG16 LN + CIFAR-10. The final test accuracy of the midpoint model is reported.

Variant	WM		AM	
	REPAIR	RESCALE	REPAIR	RESCALE
Original	89.2%	87.27%	87.95%	84.27%
Data Independent	88.39%	86.2%	86.47%	83.16%

F.3. Effect of Matching: Knowledge Retained

We present the full results of the information measure in Figures 36, 37, 38, 39, 40 and 41, including VGG16/VGG16 BN/plain ResNet20/ResNet20 (4× width) trained on CIFAR-10 and VGG11/plain ResNet20 trained on CIFAR-100. In all settings, the post-matching midpoint model rapidly recovers a training accuracy of over 90% with a good generalization, in sharp contrast to the standard training and the one without matching.

Figure 43 records the magnitude and number of zero activations in VGG16 and plain ResNet20 trained on CIFAR-10. In both cases, the usage of matching algorithms decreases the loss in weight magnitude, indicating more information being retained in the model. Regarding the hidden activations, it was observed that the original interpolated model has more zero activations in the early layers per forward calculation. We regard this as a consequence of information loss which leads to more noise in the deeper layers. This issue was alleviated after matching. Figure 35 illustrates the analogy between the pruning and linear mode connectivity.

We also evaluated standard information measures in our experiments, for instance, the Fisher Information (Fisher, 1925). Same as conventional practices (Achille et al., 2018), we calculate the diagonal estimation. Figure 42 illustrates the average Fisher Information in each layer. An obvious increase in information is also observed after both weight matching and activation matching.

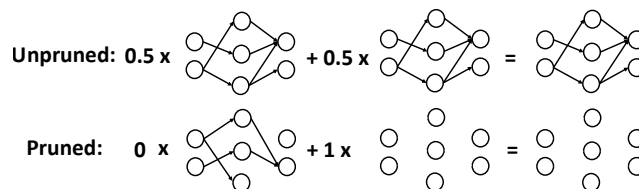


Figure 35. Interpret network pruning as a parameter-wise linear interpolation.

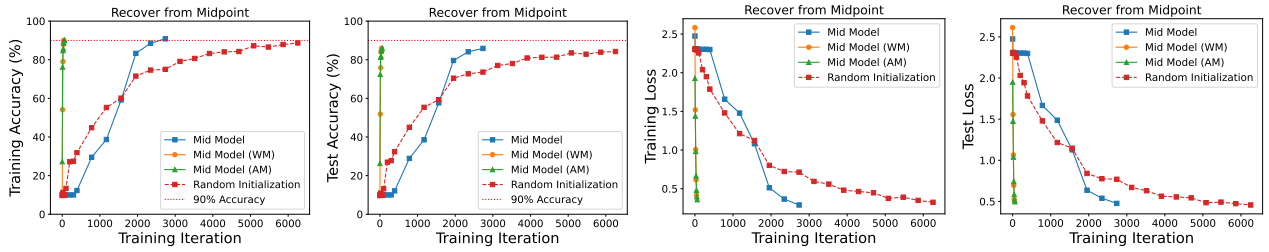


Figure 36. Recover from the midpoint, evaluated on VGG16 + CIFAR-10.

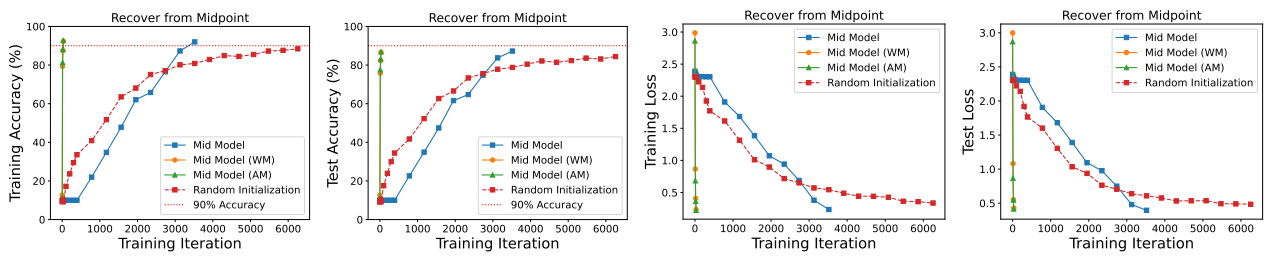


Figure 37. Recover from the midpoint, evaluated on VGG16 BN + CIFAR-10.

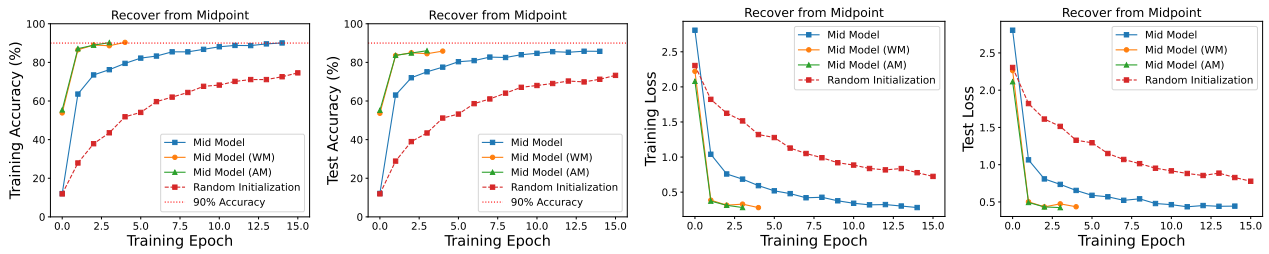


Figure 38. Recover from the midpoint, evaluated on plain ResNet20 + CIFAR-10.

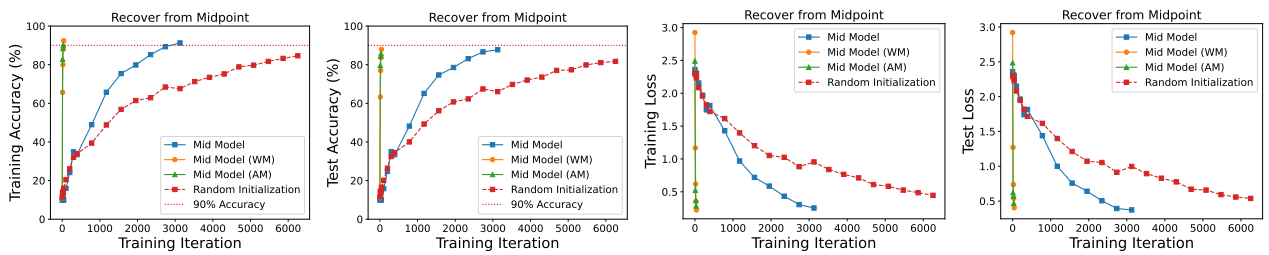


Figure 39. Recover from the midpoint, evaluated on ResNet20 (4x width) + CIFAR-10.

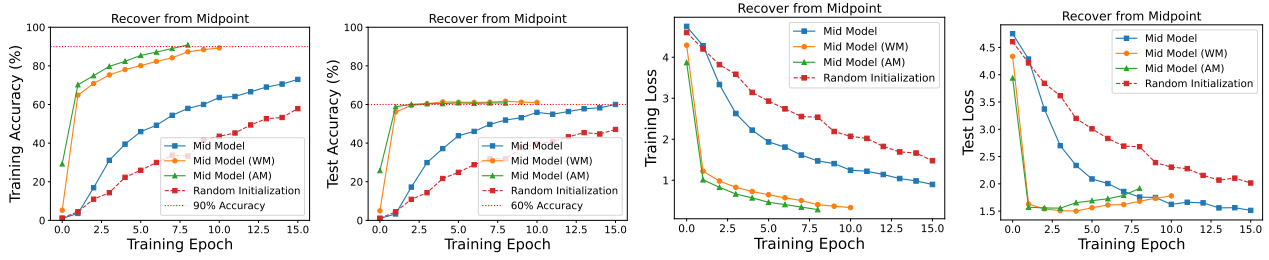


Figure 40. Recover from the midpoint, evaluated on VGG11 + CIFAR-100.

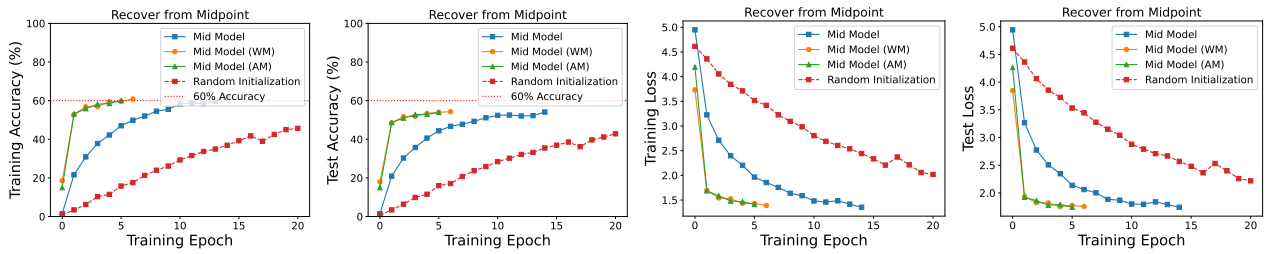


Figure 41. Recover from the midpoint, evaluated on plain ResNet20 + CIFAR-100.

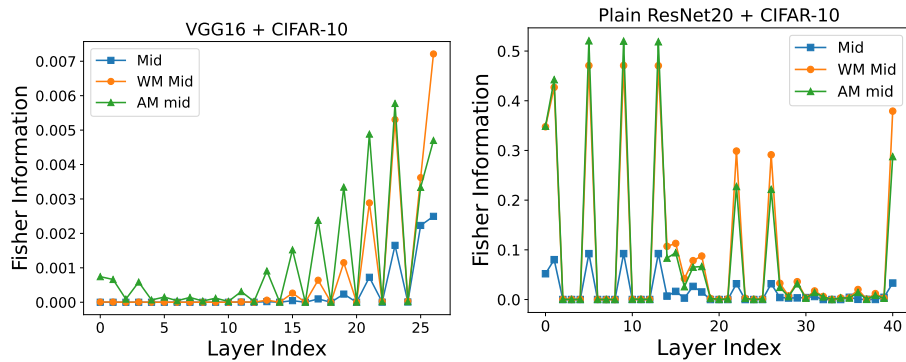


Figure 42. The average Fisher Information in each layer.

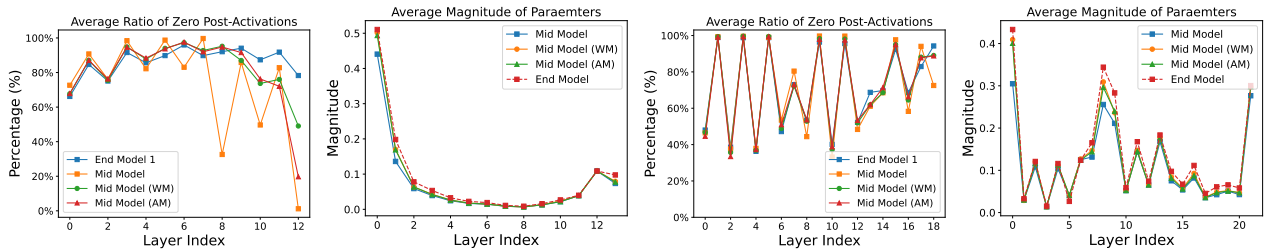


Figure 43. Percentage of zero post-activation per forward calculation and the average magnitude of parameters in each layer. **Left two:** VGG16 + CIFAR-10. **Right two:** Plain ResNet20 + CIFAR-10.

F.4. Learning Rate and Sparsity

We empirically examine the connection between learning rate and sparsity as stated in (Andriushchenko et al., 2023b) in this section. Specifically, we compare the model trained with different learning rates on performance after the fundamental global unstructured magnitude pruning. The results of VGG16 BN and ResNet20 ($4\times$ width) trained on CIFAR-10 are shown in Figure 44. In all plots, the models trained with a larger learning rate have a better performance after pruning, which is exactly consistent with the definition of sparsity utilized throughout the paper, i.e., the information is concentrated on a small fraction of important parameters.

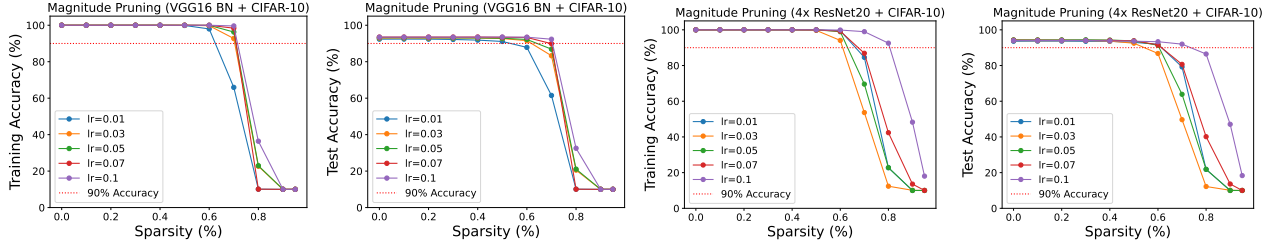


Figure 44. Global unstructured magnitude pruning.

F.5. Implicit Bias of Learning Rate

The complete results of comparing different values of learning rate are shown in Figures 45 and 46. In all settings and for both weight matching and activation matching, the barrier keeps decreasing with a larger learning rate. We also provide all the interpolation plots in Figures 47, 48, 50, 51, 53, 54, 56 and 57. The complete results of VGG16 LN + MNIST are provided in Figure 59. The effect of initialization when training with a small learning rate is illustrated in Figures 60 and 61. In particular, the same observation was drawn on ResNet20 LN. The L_2 distance during training is shown in Figure 62.

To demonstrate that the decrease in the barrier brought by larger learning rates is not a trivial consequence of the fact that training with large learning rates can slightly improve the performance of the end models, we conducted the following experiments. After obtaining two pairs of solutions, one of which was trained with large $lr = 0.1$ and the other was trained with small $lr = 0.01$, we retrained the large lr solutions with $lr = 0.1$ for one more epoch to degrade their performances. Then we compare their interpolation results with the results between small lr solutions. As illustrated in Figures 49, 52, 55, and 58, in all settings and for both weight matching and activation matching, the large lr models still outperforms regarding the midpoint accuracy, though the end models already have a worse performance at this point.

Additionally, we describe the detailed initialization strategy for VGG16 LN below. The two different strategies are also compared on ResNet20 LN. For the Kaiming uniform initialization, we directly adopted the PyTorch (Paszke et al., 2019) default. The Kaiming normal initialization is standard for training VGG, e.g., used in Torchvision. Specifically, for a 2D convolutional layer, the uniform initialization samples the weights and biases from the uniform distribution $U\left[\frac{-1}{\sqrt{k}}, \frac{1}{\sqrt{k}}\right]$, where $k = \text{num_in} \times \text{kernel_size}[0] \times \text{kernel_size}[1]$; while the normal initialization samples the weights from the Gaussian distribution $N\left(0, \frac{2}{k}\right)$, where $k = \text{num_out} \times \text{kernel_size}[0] \times \text{kernel_size}[1]$, and sets the bias to 0. For a linear layer, the uniform initialization samples weights and biases from $U\left[\frac{-1}{\sqrt{k}}, \frac{1}{\sqrt{k}}\right]$, where $k = \text{num_in}$; while the normal initialization samples the weights from $N(0, 0.01)$ and sets bias to zero. This creates a larger variance at initialization for the normal initialization, which can be observed from the distance between two independently initialized models, as illustrated in Figures 5 and 62. This significant difference in distance was observed to remain in the training when a small learning rate was utilized and affected the performance of matching.

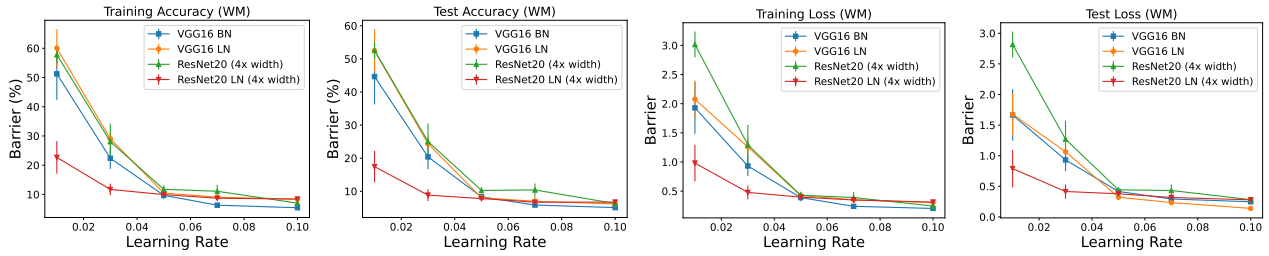


Figure 45. Barrier between two independent models trained on CIFAR-10. Weight matching is applied.

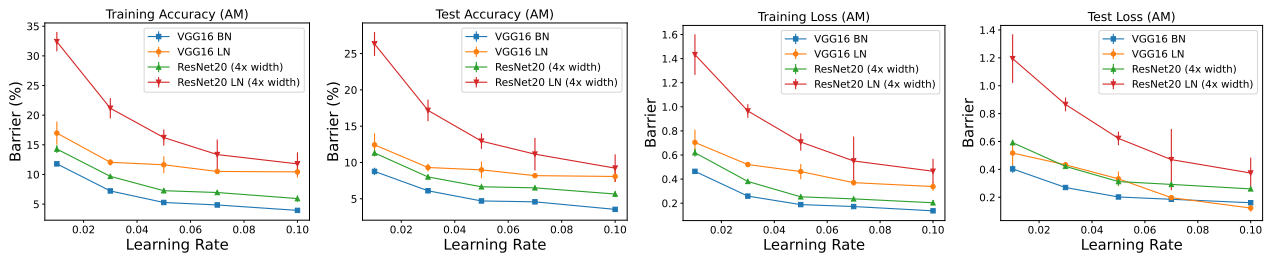


Figure 46. Barrier between two independent models trained on CIFAR-10. Activation matching is applied.

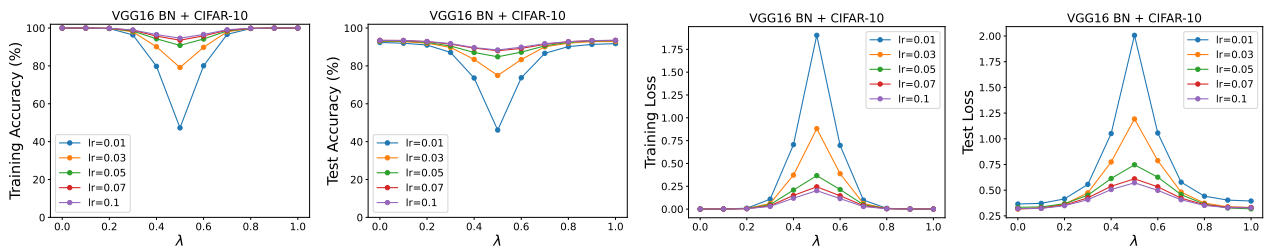


Figure 47. Benefit brought by training with large learning rates. Linear interpolation plot between two independent VGG16 BN trained on CIFAR-10. Weight matching is applied.

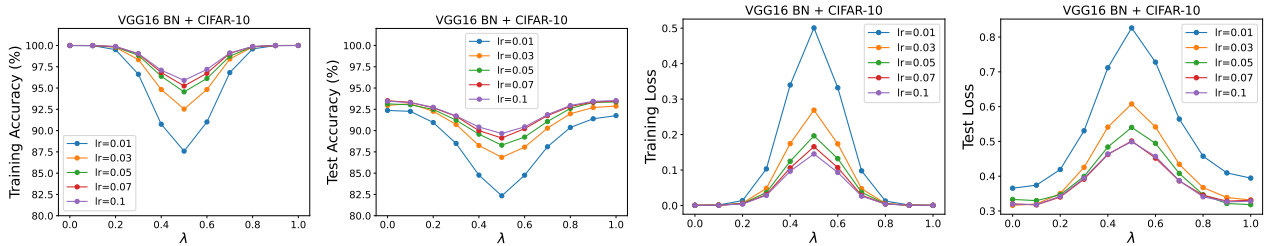


Figure 48. Benefit brought by training with large learning rates. Linear interpolation plot between two independent VGG16 BN trained on CIFAR-10. Activation matching is applied.

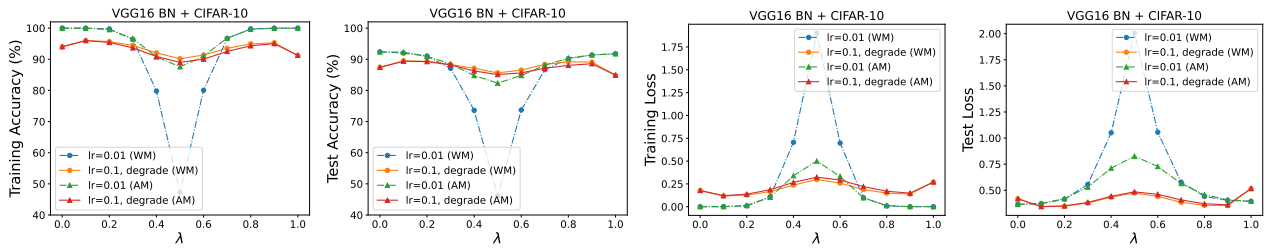


Figure 49. Learning rate ablation, VGG16 BN + CIFAR-10. The “degrade” refers to the interpolation after retraining the solution for one epoch.

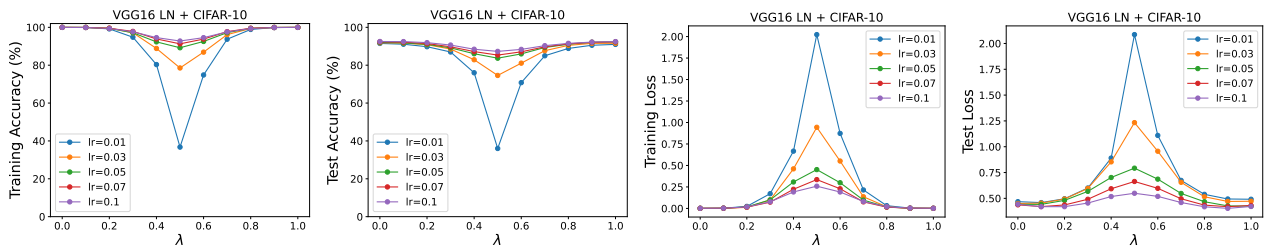


Figure 50. Benefit brought by training with large learning rates. Linear interpolation plot between two independent VGG16 LN trained on CIFAR-10. Weight matching is applied.

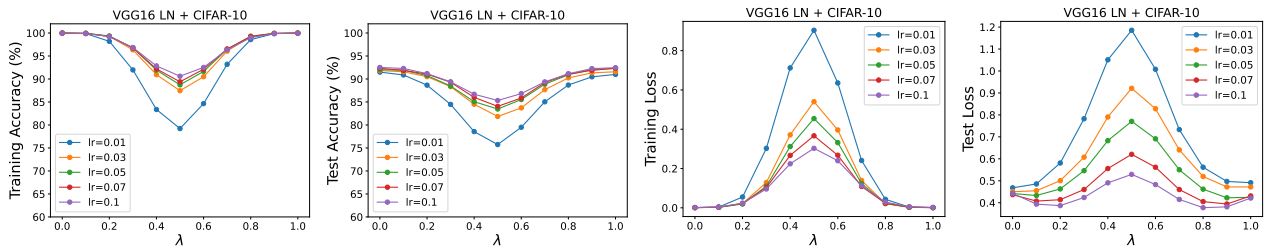


Figure 51. Benefit brought by training with large learning rates. Linear interpolation plot between two VGG16 LN trained on CIFAR-10. Activation matching is applied.

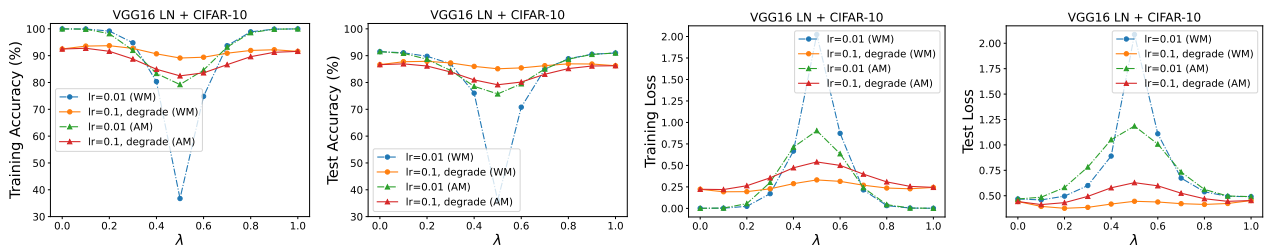


Figure 52. Learning rate ablation, VGG16 LN + CIFAR-10. The “degrade” refers to the interpolation after retraining the solution for one epoch.

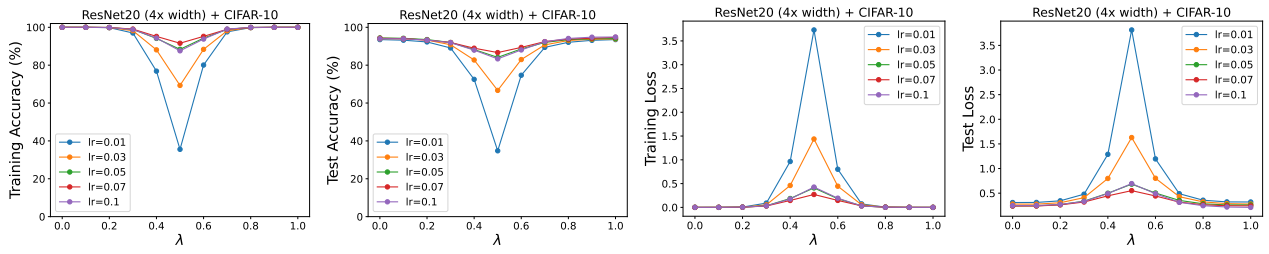


Figure 53. Benefit brought by training with large learning rates. Linear interpolation plot between two ResNet20 (4× width) trained on CIFAR-10. Weight matching is applied.

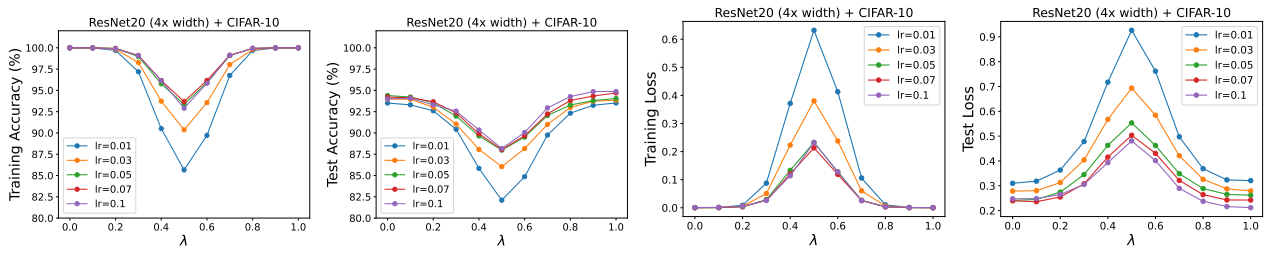


Figure 54. Benefit brought by training with large learning rates. Linear interpolation plot between two independent ResNet20 (4× width) trained on CIFAR-10. Activation matching is applied.

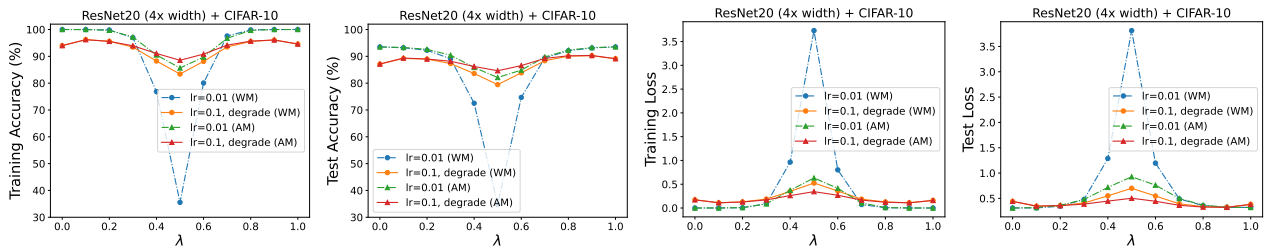


Figure 55. Learning rate ablation, ResNet20 (4× width) + CIFAR-10. The “degrade” refers to the interpolation after retraining the solution for one epoch.

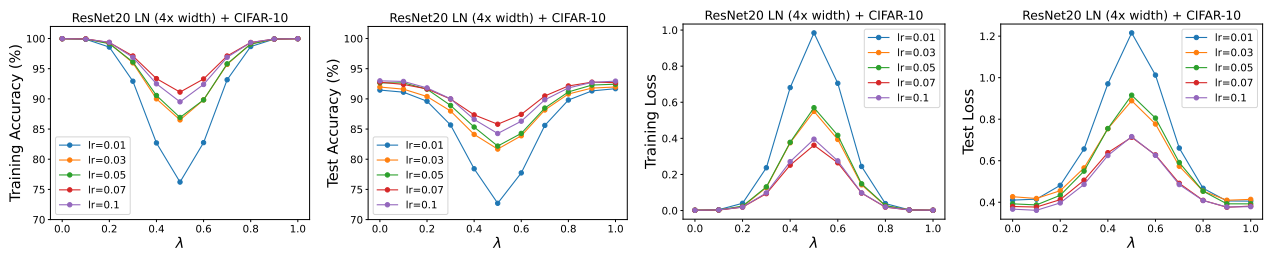


Figure 56. Benefit brought by training with large learning rates. Linear interpolation plot between two independent ResNet20 LN (4× width) trained on CIFAR-10. Weight matching is applied.

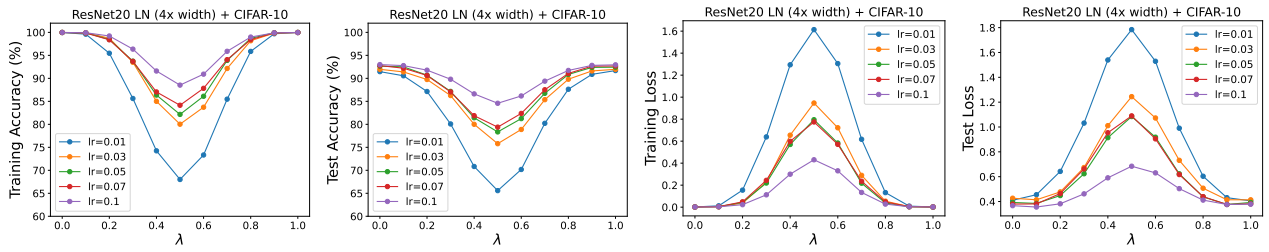


Figure 57. Benefit brought by training with large learning rates. Linear interpolation plot between two independent ResNet20 LN (4x width) trained on CIFAR-10. Activation matching is applied.

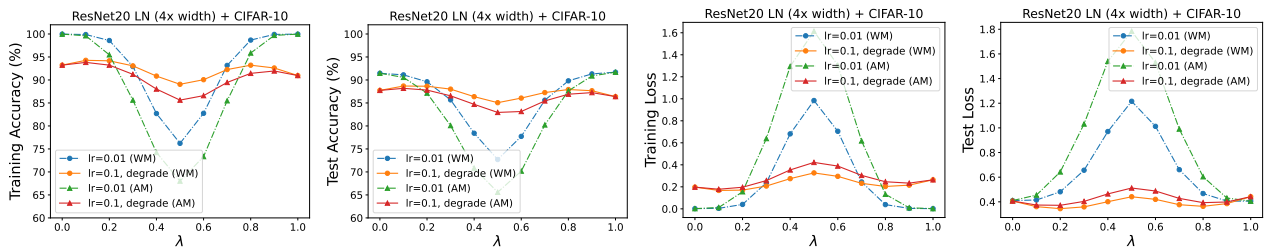


Figure 58. Benefit brought by training with large learning rates. Learning rate ablation, ResNet20 LN (4x width) + CIFAR-10. The “degrade” refers to the interpolation after retraining the solution for one epoch.

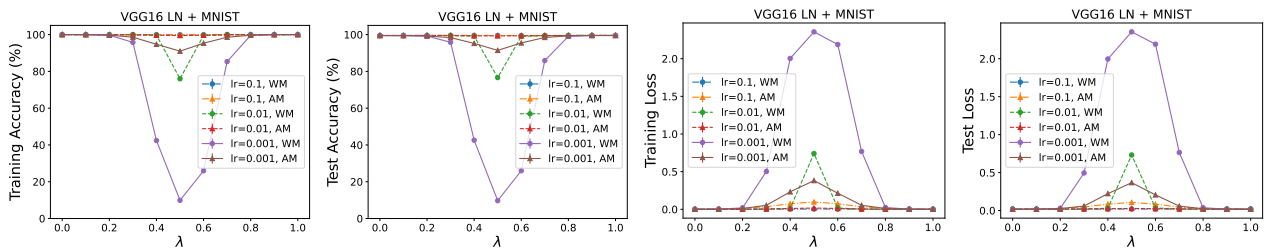


Figure 59. Linear interpolation plot between two independent VGG16 LN trained on MNIST.

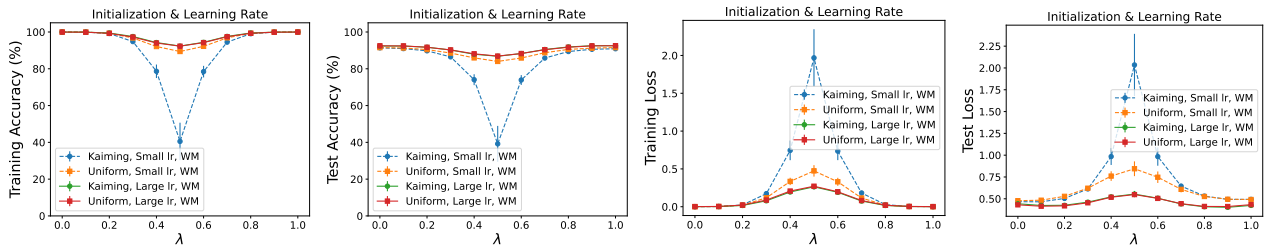


Figure 60. Sensitivity to initialization when training models with small learning rates. Linear interpolation plot between two independent VGG16 LN trained on CIFAR-10. Kaiming: Kaiming normal initialization. Uniform: Kaiming uniform initialization.

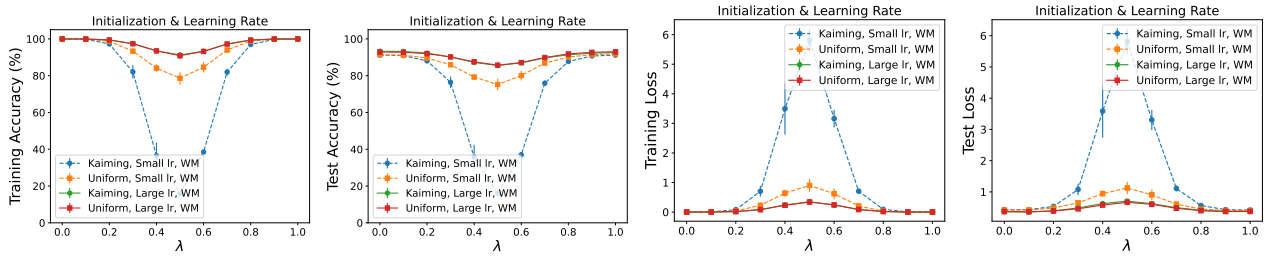


Figure 61. Sensitivity to initialization when training models with small learning rates. Linear interpolation plot between two independent ResNet20 LN ($4\times$ width) trained on CIFAR-10. Kaiming: Kaiming normal initialization. Uniform: Kaiming uniform initialization.

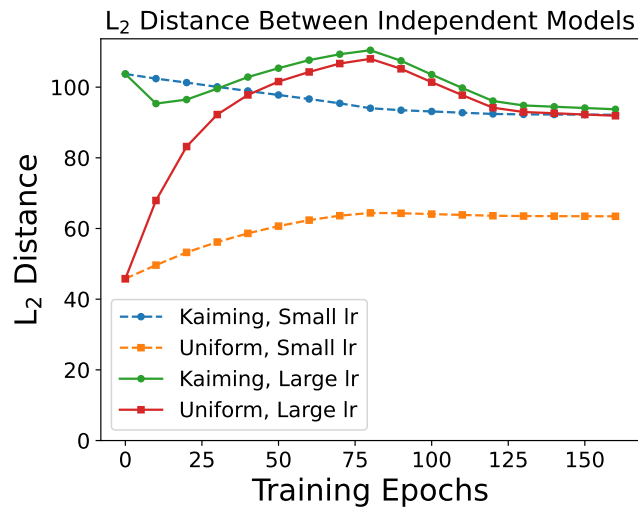


Figure 62. Distance between independent ResNet20 LN ($4\times$ width) trained on CIFAR-10. “Kaiming” refers to the Kaiming normal initialization and “Uniform” refers to the Kaiming uniform initialization.

E.6. Implicit Bias of Weight Decay

We provide the interpolation plots in Figures 63, 65, and 67. Same as Sec. F.5, we conducted the retraining experiment to validate that the benefit brought by utilizing a larger weight decay is not solely due to the improved performance of end models. Here, we retrain the small $wd = 1e - 4$ solutions for one more epoch with $wd = 5e - 4$. Results are illustrated in Figures 64, 66, and 68. Similarly, we observed that the midpoint model between larger wd models after retraining still outperforms.

We showcase the compression effect brought by weight decay regularization in Figures 69 and 70. The density plots of the parameter magnitude and activation statistics are reported. The activation statistics are averaged in each channel. Complete results of improving REPAIR by RESCALE are provided in Figure 71.

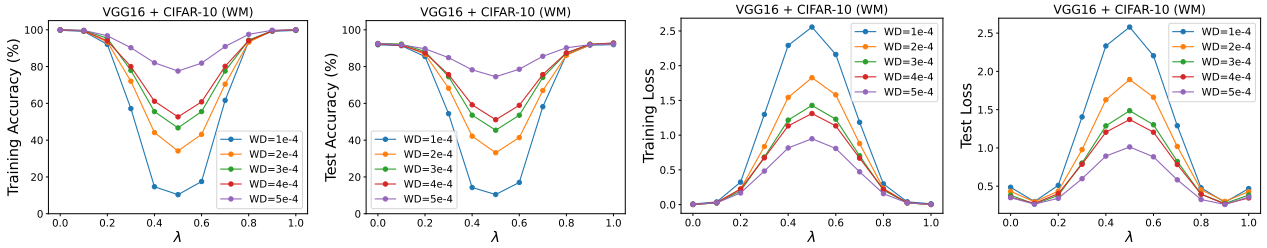


Figure 63. Benefit brought by training with large weight decay. Linear interpolation between independent VGG16 trained on CIFAR-10. Weight matching is applied.

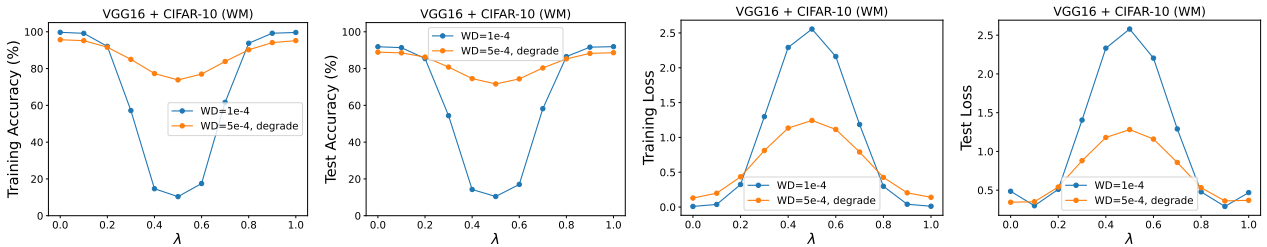


Figure 64. Weight decay ablation, VGG16 + CIFAR-10. Weight matching is applied. The “degrade” refers to the interpolation after retraining the solution for one epoch.

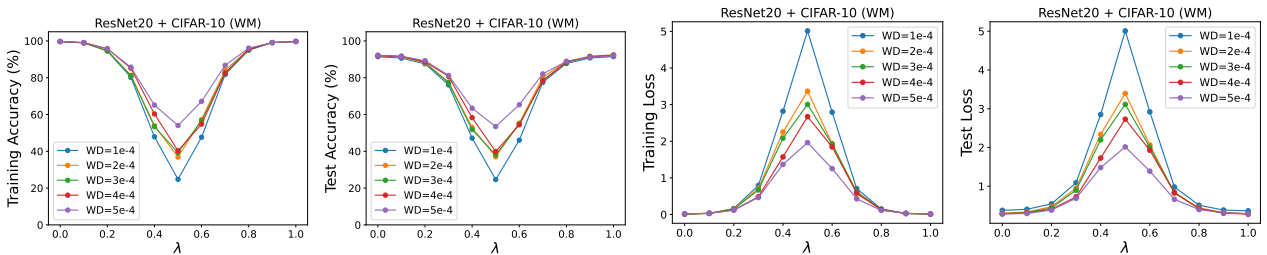


Figure 65. Benefit brought by training with large weight decay. Linear interpolation between independent ResNet20 trained on CIFAR-10. Weight matching is applied.

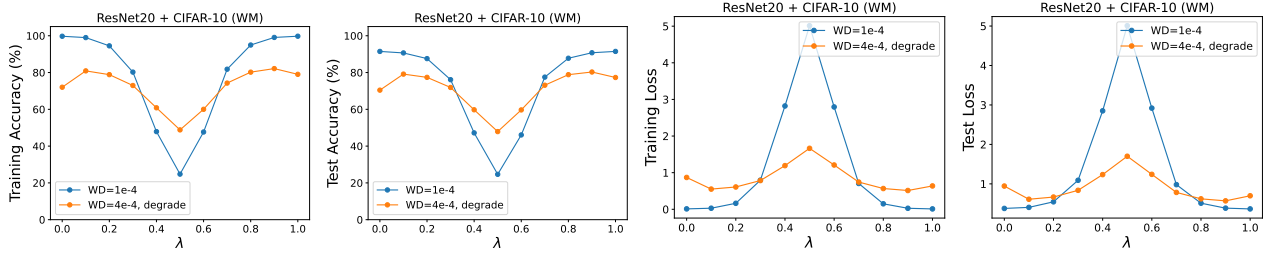


Figure 66. Weight decay ablation, ResNet20 + CIFAR-10. Weight matching is applied. The “degrade” refers to the interpolation after retraining the solution for one epoch.

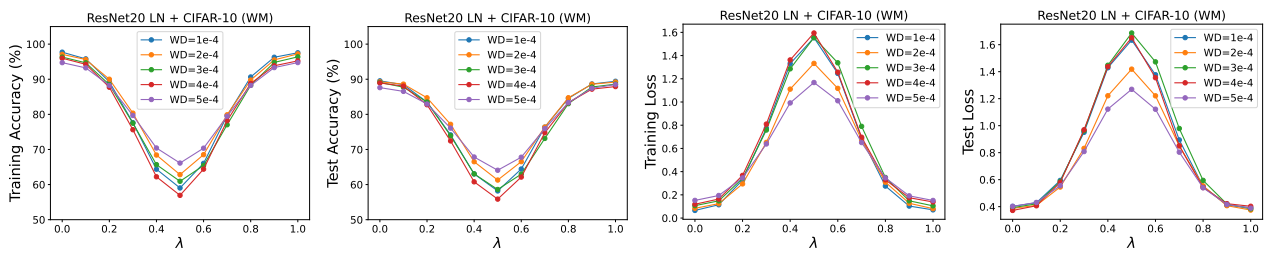


Figure 67. Benefit brought by training with large weight decay. Linear interpolation between independent ResNet20 LN trained on CIFAR-10. Weight matching is applied.

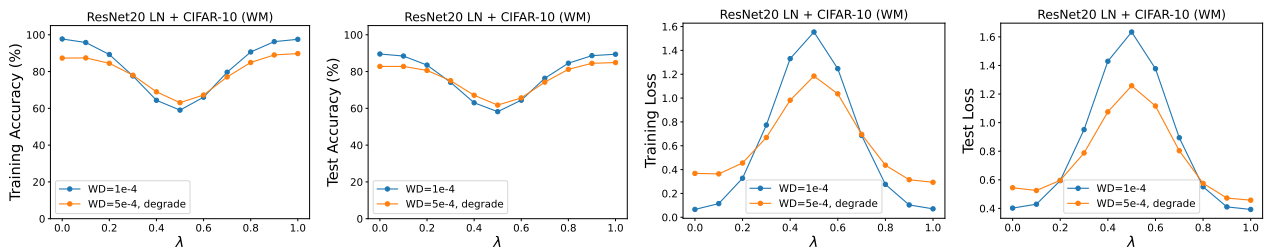


Figure 68. Weight decay ablation, ResNet20 LN + CIFAR-10. Weight matching is applied. The “degrade” refers to the interpolation after retraining the solution for one epoch.

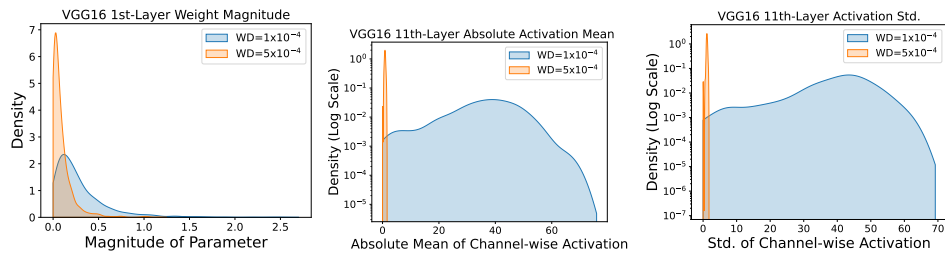


Figure 69. The compression effect brought by weight decay, VGG16 + CIFAR-10. Density plots are reported.

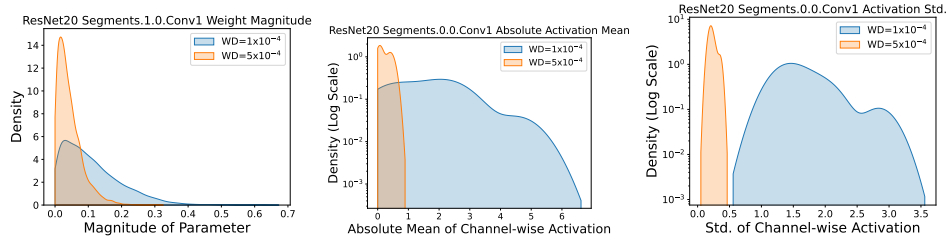


Figure 70. The compression effect brought by weight decay, ResNet20 + CIFAR-10. Density plots are reported.

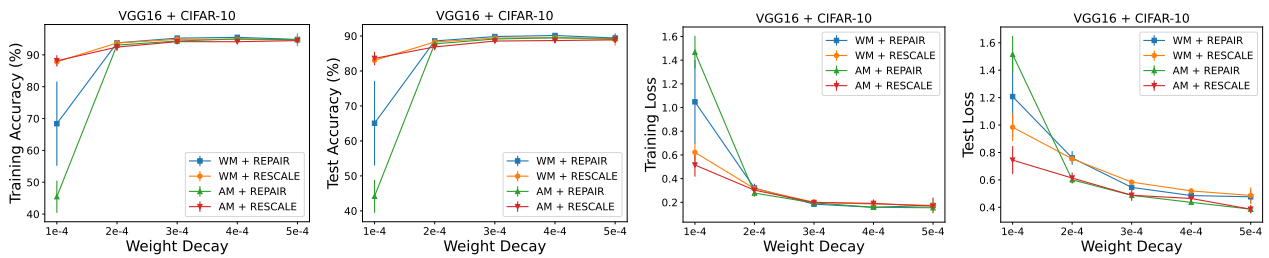


Figure 71. Improve REPAIR by RESCALE. The barrier between two VGG16 on CIFAR-10 is illustrated.

G. Supplementary to Sec. 5

We present additional results of pruning ResNet20, ResNet20 LN, VGG16 BN, VGG16 LN, and plain ResNet20 on CIFAR-10 and CIFAR-100 in Figure 72 and 73. In all experiments, we follow the standard setup of Singh & Alistarh (2020) only to prune weights in all convolutional and linear layers. The first convolutional layer is ignored when pruning ResNet50 on ImageNet. The code for all pruning experiments is adapted from Singh & Alistarh (2020) with merely several new lines of code for performing REPAIR and RESET, demonstrating the convenience when merging this technique with any existing pruning framework. Consequently, the same hyperparameters for pruning as (Singh & Alistarh, 2020) are adopted in this work. For instance, the fisher subsample size and fisher mini-batch size for the WoodFisher pruner are set to 400 in CIFAR-10/CIFAR-100 pruning. For the model except ResNet50, results with sparsity rates of 10%, 20%, . . . , 90%, 95%, and 99% are reported. For ResNet50, we prune the model up to a sparsity of 90%. Since the main objective of this work is not to highlight this novel post-pruning technique, we only demonstrate its power in the one-shot pruning scenario, but the logic also applies to other pruning frameworks, such as structured pruning and gradual pruning. We regard this as a promising direction worthy of further exploration and leave this for future work. For pruning ResNet50 on ImageNet, a simple hyperparameter setting of the WoodFisher pruner is utilized, e.g., fisher subsample size = 80 and fisher mini-batch size = 100, to save computational cost. Although this restricts the performance of the pruner, a significant improvement after RESET is already demonstrated in our results and should be universal after merely changing some hyperparameters. We leave the efforts towards improving the SOTA results for future work. Meanwhile, we noticed that the RESET in models with BatchNorm was already used in a few pruning literature (Li et al., 2020), but its direct impact on improving the final model performance hasn't been thoroughly investigated. We emphasize that, for instance, the significant improvement in one-shot pruning is valuable in cases where the local re-training is not able to proceed, e.g., in some end devices in the context of federated learning (McMahan et al., 2017). Furthermore, the usage of REPAIR in our work makes it possible to apply this strategy to a wider range of model architectures.

In Jordan et al. (2022), it was reported that feeding a small portion of data ($\sim 5,000$ examples) for statistics recording is already sufficient to guarantee the performance of REPAIR/RESET. In the context of pruning, we found that even one batch of data (64 in our pruning experiment) is often already enough. We provide one example of applying RESET with 64/128/258 samples to the pruned ResNet20 on CIFAR-10 in Figure 74. Note that this is both for the statistics recording in the unpruned model and the pruned model. For both global magnitude pruning and layerwise magnitude pruning, one batch of data already suffices to produce a result almost the same as the complete RESET. This is particularly meaningful in resource-limited settings, especially considering its remarkable performance-boosting ability, which can yield comparable results to advanced pruning methods like WoodFisher, even when applied to simple magnitude pruning. It's also noteworthy that the additional BN parameters in REPAIR can be eliminated by merging them into the original layers, as discussed in the original paper (Jordan et al., 2022). In summary, this re-normalization technique is extremely lightweight as there are no additional parameters, and the computational cost is negligible.

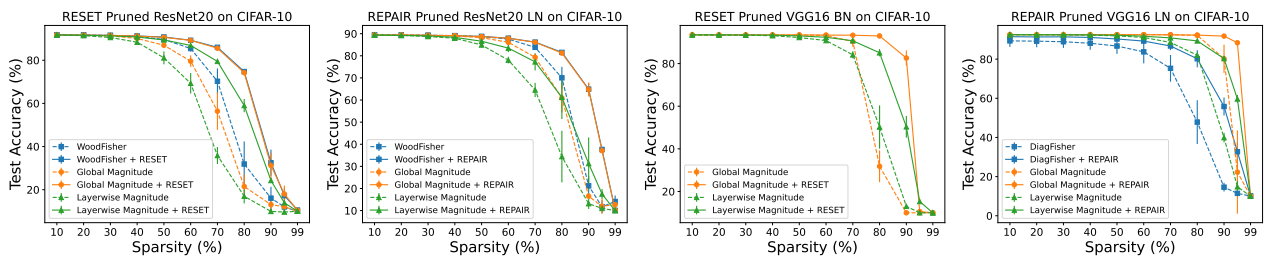


Figure 72. Apply REPAIR/RESET to pruned models on CIFAR-10. The diagonal-Fisher pruning performs poorly on VGG16 BN and is hence ignored here.

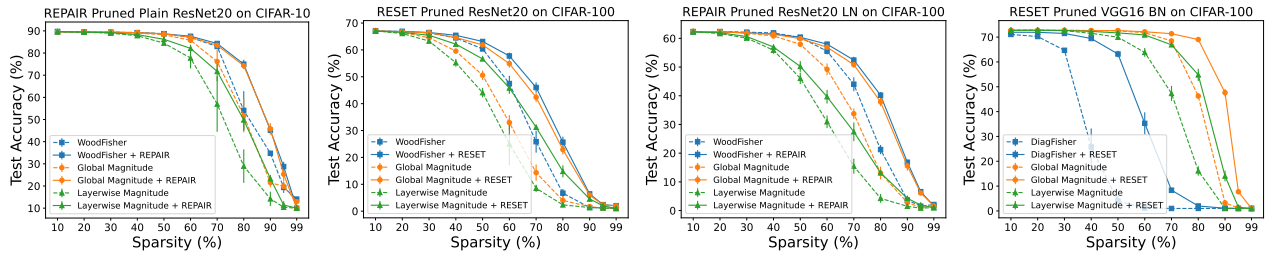


Figure 73. (A) Apply REPAIR to pruned plain ResNet20 on CIFAR-10. (B) & (C) & (D) Apply RESET/REPAIR to pruned models on CIFAR-100.

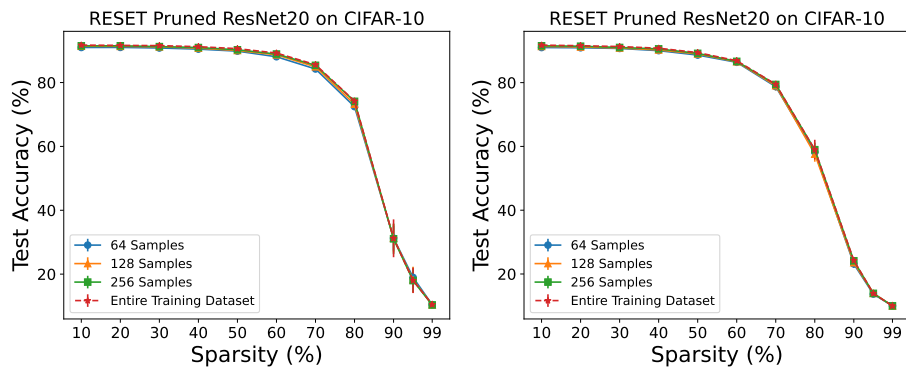


Figure 74. Compare the number of samples utilized in re-normalization. **Left:** Global magnitude pruning. **Right:** Layerwise magnitude pruning.